Monthly Notices of the ROYAL ASTRONOMICAL SOCIETY

MNRAS **00,** 1 (2023) https://doi.org/10.1093/mnras/stad050
Advance Access publication 2023 January 9

ExoMol line lists – L: high-resolution line lists of H_3^+, H_2D^+, D_2H^+, and D_3^+

Charles A. Bowesman,[1] Irina I. Mizus,[2,3] Nikolay F. Zobov,[3] Oleg L. Polyansky,[1,3] János Sarka,[4,5] Bill Poirier,[4] Marco Pezzella,[1] Sergei N. Yurchenko [1] and Jonathan Tennyson [1]★

[1]*Department of Physics and Astronomy, University College London, Gower Street, WC1E 6BT London, UK*
[2]*Holon Institute of Technology, Golomb Street, 52, Holon 5810201, Israel*
[3]*Institute of Applied Physics, Russian Academy of Science, Ulyanov Street 46, Nizhnii Novgorod 603950, Russia*
[4]*Department of Chemistry and Biochemistry, Texas Tech University, Lubbock, TX 79409, United States*
[5]*Institute of Chemistry, Eötvös Loránd University, Budapest, Hungary*

Accepted 2022 December 29. Received 2022 December 24; in original form 2022 November 15

ABSTRACT

New MiZo line lists are presented for the D_2H^+ and D_3^+ isotopologues of H_3^+. These line lists plus the existing H_3^+ MiZATeP and the Sochi H_2D^+ line lists are updated using empirical energy levels generated using the MARVEL procedure for H_3^+, H_2D^+, and D_2H^+, and effective Hamiltonian energies for D_3^+ for which there is significantly less laboratory data available. These updates allow accurate frequencies for far infrared lines for these species to be predicted. Assignments of the energy levels of H_3^+ and D_3^+ are extended using a combination of high accuracy variational calculations and analysis of transition intensities. All line lists are made available via www.exomol.com.

Key words: molecular data – opacity – planets and satellites: atmospheres – stars: atmospheres – ISM: molecules.

1 INTRODUCTION

H_3^+ is known to form rapidly in H_2 gas following an ionization event via the strongly exothermic reaction

$$H_2 + H_2^+ \longrightarrow H_3^+ + H, \quad (1)$$

which occurs at essentially every collision. As H_2 is common in a variety of astronomical bodies, H_3^+ is often the dominant molecular ion. The first 30 yr of H_3^+ astronomy has been comprehensively reviewed by Miller et al. (2020). H_3^+ formation is stimulated by cosmic ray ionization of the interstellar medium and by collisions with fast electrons and other charged particles in planetary ionospheres. H_3^+ is also believed to form in the ionosphere of planets through the ionization of H_2 by extreme ultraviolet radiation (Chadney et al. 2016). In gas giant ionospheres, H_3^+ acts as a coolant through efficient infrared (IR) emissions (Miller et al. 2010); indeed, it is thought that H_3^+ emissions are key to determining the stability limits in hot Jupiter exoplanets (Koskinen, Aylward & Miller 2007).

The infrared spectrum of H_3^+ has been extensively observed in giant planets in our Solar system such as Jupiter (Drossart et al. 1989; Ballester et al. 1994; Miller et al. 1997; Moore et al. 2017), Saturn (Geballe, Jagod & Oka 1993; Stallard et al. 2008a, b), Uranus (Trafton et al. 1993; Lam et al. 1997; Trafton et al. 1999; Melin et al. 2019), and is believed to be present in Neptune (Melin et al. 2011, 2018) although it is yet to be detected there. Its presence can be used as an effective temperature probe here and in other astrophysical settings (Gibbs & Fitzgerald 2022). H_3^+ is similarly expected to be of importance in extrasolar giant planets (Chadney et al. 2016; Khodachenko et al. 2015), such as hot Jupiters (Lenz et al. 2016), and an even more prominent feature in the aurorae of brown dwarfs (Gibbs & Fitzgerald 2022); however, it has so far defied observation on these objects.

H_3^+ has also been observed in the interstellar medium (ISM) via absorption in the infrared light of a background star (Oka 2006) where it forms through cosmic ray ionization (Geballe & Oka 1996). Hence, it is also used in this setting to trace the cosmic ray ionization rate (Indriolo & McCall 2012; Harju et al. 2017) and similarly primarily relies on IR emissions. These IR bands lie well within the wavelength range of the instruments onboard the JWST.

In regions where the precursors to H_3^+ exist in deuterated forms, namely HD and D_2, equivalent reactions occur to that described in equation (1) resulting in the formation of the deuterated isotopologues H_2D^+, D_2H^+, and D_3^+ (Merkt, Hoeveler & Deiglmayr 2022). At low temperatures, fractionation drives the preferential formation of isotopically substituted H_3^+ (Hewitt et al. 2005); indeed, models by Walmsley, Flower & des Forets (2004) suggest that in certain very cold regions D_3^+ may be the dominant isotopologue of H_3^+! Spectra of H_2D^+ (Stark, van der Tak & van Dishoeck 1999; Caselli et al. 2003) and D_2H^+ (Vastel, Phillips & Yoshida 2004) have been observed in interstellar space through pure rotational transitions which lie in the far infrared/THZ region. However, D_3^+ remains undetected, at least in part because its higher symmetry means that, like H_3^+, its pure rotational spectrum is very weak. Elsewhere, electrons provided by H_3^+ have been shown to play an important role in the atmospheres of cool white dwarfs (Bergeron, Ruiz & Leggett 1997).

Line lists for H_3^+ (Kao et al. 1991; Neale, Miller & Tennyson 1996) and the associated partition function (Neale & Tennyson 1995; Ramanlal & Tennyson 2004) have played a key role in the astronomical study of this important molecular ion. In this work,

★ E-mail: j.tennyson@ucl.ac.uk

we update the MiZATeP H_3^+ line list of Mizus et al. (2017) and the older ST1 H_2D^+ line list of Sochi & Tennyson (2010). We do this using updated versions of the MARVEL (measured active rotation-vibration energy levels) studies due to Furtenbacher et al. (2013a, b). We present new line lists for D_2H^+ and D_3^+, for which, we also use empirical energy levels to improve the accuracy of the transition frequencies between key levels. These line lists are produced as part of the ExoMol project (Tennyson & Yurchenko 2012).

2 METHOD

The triatomic discrete variable representation (DVR) nuclear motion code DVR3D (Tennyson et al. 2004) was used previously and here to compute initial energy levels for H_3^+ and its deuterated isotopologues as well as Einstein A-coefficients for each transition. This code, which is based on the use of an exact nuclear motion kinetic energy operator, has been shown to be capable of giving highly accurate results for the H_3^+ system (Polyansky & Tennyson 1999; Pavanello et al. 2012a). It is important to note that in the absence of any absolute measurements of transition intensities for the H_3^+ system, all models rely on computed values which are thought to be accurate (Farnik et al. 2002; Petrignani et al. 2014). It should be noted that DVR3D only provides assignments for the rigorous quantum numbers: J, rotationless parity *e*/*f* and the interchange symmetry for two identical atoms. This means that most states in the existing version of the MiZATeP H_3^+ (Mizus et al. 2017) and ST1 H_2D^+ (Sochi & Tennyson 2010) line lists do not have full ro-vibrational labels. We partially address this issue below.

MARVEL (Furtenbacher, Császár & Tennyson 2007; Furtenbacher & Császár 2012; Tóbiás et al. 2018) takes assigned high resolution spectra and uses them to construct empirical energy levels with spectroscopic accuracy and specified uncertainties. Use of the energy levels can greatly improve the accuracy with which a line list can predict transition frequencies (see Al-Derzi et al. 2021 for a recent example). For H_3^+, H_2D^+, and D_2H^+, MARVEL spectroscopic networks were then constructed using available laboratory spectra in order to obtain empirical energy levels for each species. These empirical energy levels were then used to improve our line lists, correcting for obs.–calc. shifts in levels where empirical energy levels are available for comparison. Such a refinement allows for a subset of the energies to be provided with very high accuracy, as has been demonstrated in similar projects (Bowesman et al. 2022). This allows for high-accuracy transition frequency predictions to be made (Al-Derzi et al. 2021), making the final line list well suited for high-resolution studies (Bowesman et al. 2021; Owens et al. 2022).

The MARVEL process determines an uncertainty for each energy level based on the uncertainties of the input transition that define that level.

2.1 Spectroscopic networks

Transition data for a molecule can be aggregated to construct a spectroscopic network, where the transition frequencies represent the edges of the networks and the energy levels the nodes (Furtenbacher et al. 2007; Császár & Furtenbacher 2011). The MARVEL procedure (Furtenbacher & Császár 2012) achieves this by inverting transition matrices, which yields a set of empirical energy levels with individual uncertainties. Spectroscopic networks have been constructed in the past for the molecules H_3^+ (Furtenbacher et al. 2013a), H_2D^+, and D_2H^+ (Furtenbacher et al. 2013b) but new transition data has since been published. New transition data allow us to expand the level coverage of the networks and in the case of new data that remeasures existing transitions to improve the accuracy to which term energies are known. The recent high-resolution experiments have provided new THz transition data with uncertainties on the order of MHz or kHz, well within the part-per-billion regime. When all of the transitions that determine a level's term energy are consistent within their experimental uncertainties, the uncertainty on the final term energy will generally be on the same order, but not less than the smallest uncertainty of the transitions that define the level. Hence, with the addition of these high-accuracy transition measurements, we are able to significantly improve the accuracy of our final energies, in some cases by a few orders of magnitude.

Table 1. The rovibronic symmetries of the isotopologues of H_3^+ where g_{ns} is the nuclear spin statistical weight. For H_3^+ and D_3^+, Γ_{rve} are representations of the D_{3h} point group, while for H_2D^+ and D_2H^+, they are for C_{2v}.

Γ_{rve}	Isomer	g_{ns}	Isomer	g_{ns}
	H_3^+		D_3^+	
A_1', A_1''	–	0	ortho	10
A_2', A_2''	ortho	4	para	1
E', E''	para	2	meta	8
	H_2D^+		D_2H^+	
A_1, A_2	para	3	ortho	12
B_1, B_2	ortho	9	para	6

The MARVEL procedure requires all transitions within a network to be identified by the same set of quantum numbers. For this purpose, the deuterated isotopologues can be divided into two groups: H_3^+ and D_3^+ are symmetric-tops belonging to the D_{3h}(M) molecular symmetry group and H_2D^+ and D_2H^+ are asymmetric-tops belonging to the C_{2v}(M) group. These in turn dictate the set of good quantum numbers used to define the levels of the networks.

As symmetric tops, the molecules H_3^+ and D_3^+ are defined by two primary vibrational modes, symmetric stretching (ν_1) and bending (ν_2). The bending mode is degenerate however, and as such these species are also described by the vibrational angular momentum quantum number $l_2 = \nu_2, \nu_2 - 2, ..., -\nu_2 + 2, -\nu_2$. The energy levels of these species are identified instead by $L_2 = |l_2|$ in this work. The rigorous rotational angular momentum quantum number J is used to define the rotational levels of these molecules. The projection of J along the molecular symmetry axis, k can be used to determine the parity of the energy levels, such that the total parity is the sign of $(-1)^k$ (Furtenbacher et al. 2013a). The quantum number k does not offer a complete description of the system however, due to Coriolis coupling between it and l_2. As such, the value $G = |g|$ is used, where $g = k - l_2$ (Hougen 1962). This quantum number is important because, as members of the D_{3h}(M) symmetry group, the A_1', A_1'', A_2', A_2'' rovibronic symmetries only exist for these molecules when $G = 3n$, where n is an integer. In H_3^+, the A_1' and A_1'' symmetries do not exist however, as they are determined to have 0 nuclear spin statistical weight (Watson 1984). This difference arises from the nuclear spin I of constituent atoms, which are $I = \frac{1}{2}$ for hydrogen and $I = 1$ for deuterium. Consequently H_3^+ consists of two nuclear spin isomers while D_3^+ has three (Watson, Foster & McKellar 1987); these are shown in Table 1.

Levels with equivalent vibrational, J and G assignments are differentiated by the $(u|l|m)U$-notation of Watson (1994). u and l are used to identify the upper and lower energy levels of the same assignment, differing in their value of $K = |k|$, and m is used when such a distinction is irrelevant as only one value of K can exist that produces the same G. As such, the energy levels of the species H_3^+

Table 2. The new transition assignments for transitions from the literature that previously had no assignment or were missing an upper state assignment. Assignments to transitions from Lindsay et al. (2001) were determined through comparison between the empirical energy levels determined by MARVEL, while transitions from Morong, Gottfried & Oka (2009) were assigned based on assignments produced using the code SCALIT (Sarka & Poirier 2022).

Wavenumber (cm^{-1})	v_1'	v_2'	L_2'	J'	G'	U'	K'	Γ'_{rve}	v_1''	v_2''	L_2''	J''	G''	U''	K''	Γ''_{rve}	Source
3104.125(10)	2	0	0	6	1	m	1	E''	1	0	0	6	2	m	2	E'	Lindsay et al. (2001)
3182.605(5)	1	2	2	5	2	u	0	E'	0	2	0	5	1	m	1	E''	Lindsay et al. (2001)
3235.521(5)	1	2	2	7	5	u	3	E''	1	1	1	6	5	l	6	E'	Lindsay et al. (2001)
10329.307(10)	0	4	2	7	3	u	1	A_2''	0	0	0	6	6	m	6	A_2'	Morong et al. (2009)
10462.405(10)	0	5	1	5	6	m	5	A_2''	0	0	0	6	6	m	6	A_2'	Morong et al. (2009)
10496.287(10)	2	2	2	6	8	m	6	E'	0	0	0	5	5	m	5	E''	Morong et al. (2009)
10573.997(10)	0	4	4	5	0	m	4	A_2'	0	0	0	4	3	m	3	A_2''	Morong et al. (2009)
10639.058(10)	0	5	1	5	0	m	1	A_2''	0	0	0	5	0	m	5	A_2'	Morong et al. (2009)
10666.604(10)	0	5	1	5	3	l	4	A_2'	0	0	0	5	3	m	3	A_2''	Morong et al. (2009)
10827.764(10)	0	6	0	3	0	m	0	A_2'	0	1	1	2	0	m	1	A_2''	Morong et al. (2009)
11036.111(10)	0	5	1	7	6	l	7	A_2''	0	0	0	6	6	m	6	A_2'	Morong et al. (2009)
11046.569(10)	0	5	1	6	5	l	6	E'	0	0	0	5	5	m	5	E''	Morong et al. (2009)
11048.996(10)	0	5	1	5	4	l	5	E''	0	0	0	4	4	m	4	E'	Morong et al. (2009)
11114.628(10)	2	2	2	6	3	u	1	A_2''	0	0	0	5	0	m	5	A_2'	Morong et al. (2009)
11265.189(10)	1	5	3	3	0	m	3	A_2''	0	1	1	2	3	m	2	A_2'	Morong et al. (2009)
11331.112(10)	0	5	5	5	0	m	5	A_2''	0	0	0	6	6	m	6	A_2'	Morong et al. (2009)
11556.914(10)	0	5	3	5	3	m	0	A_2'	0	0	0	4	3	m	3	A_2''	Morong et al. (2009)
11947.074(10)	2	3	1	5	6	m	5	A_2''	0	0	0	6	6	m	6	A_2'	Morong et al. (2009)
12116.353(10)	0	6	0	3	3	m	3	A_2''	0	0	0	3	0	m	0	A_2'	Morong et al. (2009)
12331.180(10)	1	4	0	5	0	m	0	A_2'	0	0	0	4	3	m	3	A_2''	Morong et al. (2009)
12502.614(10)	0	6	2	2	0	m	2	A_2'	0	0	0	3	3	m	3	A_2''	Morong et al. (2009)
12536.621(10)	1	4	2	4	3	m	1	A_2''	0	0	0	3	0	m	0	A_2'	Morong et al. (2009)
13056.013(10)	0	6	2	2	3	m	1	A_2''	0	0	0	1	0	m	0	A_2'	Morong et al. (2009)
13597.367(10)	0	6	4	1	3	m	1	A_2''	0	0	0	1	0	m	0	A_2'	Morong et al. (2009)
13676.446(10)	0	7	1	1	0	m	1	A_2''	0	0	0	1	0	m	0	A_2'	Morong et al. (2009)

and D_3^+ are identified by the quantum number set (v_1, v_2, L_2, J, G, U, K, Γ_{rve}).

As asymmetric tops, H_2D^+ and D_2H^+ are defined by the symmetric stretching, bending, and antisymmetric stretching vibrational quantum numbers v_1, v_2, and v_3. The quantum number J and its projections onto the C_2 axis and the axis perpendicular to the C_2 axis in the plane of the molecules, K_a and K_c, are the standard ones for labelling the rotational states of an asymmetric top.

For both asymmetric tops, the total parity is the sign of $(-1)^{K_c}$. A similar expression is used to identify the spin isomers of each asymmetric top, such that they are labelled ortho when it is positive and para when negative. For H_2D^+, this expression is $(-1)^{v_3+K_a}$ and for D_2H^+, it is $(-1)^{v_3+K_a+K_c}$. The ortho and para nuclear spin isomers identify the rovibronic symmetry group of the molecule, A_1, A_2, B_1, or B_2, as shown in Table 1. Hence, the energy levels of the species H_2D^+ and D_2H^+ are identified by the quantum number set (v_1, v_2, v_3, J, K_a, K_c, Γ_{rve}).

Transitions between nuclear spin isomers are forbidden, meaning networks constructed from observational transitions will be split into separate components for each isomer. Given MARVEL determines the energies of each level relative to the lowest energy level in the network, which is defined as 0, this presents a problem as any levels of a different nuclear spin isomer to that of the zero-energy level will not have their energies defined. This is avoided by the introduction of 'magic' numbers; forbidden transitions are added to the networks to connect the lowest levels of each nuclear spin isomer to each other using calculated energies. This enables the determination of all energies for connected levels within the networks, relative to the zero-energy level. For D_3^+, this treatment was not needed as the energies were determined through the use of effective Hamiltonian calculations.

2.1.1 H_3^+ network

Furtenbacher et al. (2013a) conducted a MARVEL study of H_3^+ which combined transition data from 26 sources into a single network. Since then, five new sets of high-accuracy spectra have been reported (Berg, Wolf & Petrignani 2012; Hodges et al. 2013; Perry et al. 2015; Jusko et al. 2016; Guan et al. 2018; Markus & McCall 2019) and are detailed below:

12BeWoPe (Berg et al. 2012): 3 R-branch transitions in the visible region are provided that had not been included from other sources.

13HoPeJeSi (Hodges et al. 2013): 10 R-branch transitions in the v_2 band with MHz and sub-MHz accuracy are reported. All of these transitions had been previously reported in other sources (Oka 1981; McKellar & Watson 1998), but are presented here at higher accuracy.

15PeHoMaKo (Perry et al. 2015): A further 10 R-branch transitions in the v_2 band are reported with MHz and sub-MHz accuracy. All of the transitions from this source had been observed previously (Oka 1981; Lindsay, Rade & Oka 2001; Wu et al. 2013).

16JuKoScAs (Jusko et al. 2016): 5 measurements of low-J R-branch transitions in the v_2 band are provided, all with sub-MHz accuracy. These transitions had also been observed by *13HoPeJeSi* (Hodges et al. 2013).

Table 3. The components of the updated H_3^+ MARVEL network. The network is broken down by the transition data sources and the vibrational bands contained within them, given in the form ν_1', ν_2', L_2' - ν_1'', ν_2'', L_2''. For each band, the transition energy and total angular momentum J ranges are provided, along with the mean and maximum uncertainties for these transitions. The total number of transitions validated and accessed by MARVEL (V/A) are also provided.

Vib.	J range	V/A	Energy range (cm^{-1})	Uncertainty Mean/Max (cm^{-1})
80Oka (Oka 1980)				
011–000	0–4	14/15	2457–2918	0.013/0.015
81Oka (Oka 1981)				
011–000	0–6	27/30	2457–3030	0.010/0.010
84WaFoMcBe (Watson et al. 1984)				
011–000	0–7	46/46	2217–3030	0.010/0.010
84WaFoMcBe_CD (Watson et al. 1984)				
000–000	1–4	5/5	173–596	0.010/0.012
87MaMaMcJo (Majewski et al. 1987)				
011–000	0–10	110/113	1798–3193	0.010/0.020
89MaFeWaMi (Majewski et al. 1989)				
022–000	1–12	44/50	4540–5094	0.017/0.041
90BaReOk (Bawendi et al. 1990)				
011–000	3–9	14/14	2468–2889	0.010/0.010
020–011	1–6	14/14	2395–2685	0.010/0.010
022–011	0–8	68/68	2090–2945	0.010/0.040
111–011	5–6	2/2	2741–2854	0.010/0.010
111–100	1–4	21/21	2089–2771	0.010/0.010
90NaItSuTa (Nakanaga et al. 1990)				
011–000	0–3	11/12	2457–2762	0.010/0.010
90XuGaOk (Xu et al. 1990)				
022–000	1–10	34/34	4557–5094	0.011/0.040
91LeVeCaOk (Lee et al. 1991)				
031–000	1–5	3/4	6866–6878	0.012/0.017
92XuRoGaOk (Xu et al. 1992)				
011–000	5–13	30/30	2419–3291	0.010/0.014
022–011	3–7	9/10	2893–3215	0.010/0.010
022–100	6–7	1/1	2980–2980	0.010/0.010
100–000	4–7	9/9	2454–3282	0.010/0.010
111–011	0–6	21/21	2437–3229	0.010/0.010
120–022	4–5	1/1	2990–2990	0.010/0.010
211–111	2–3	1/1	3006–3006	0.010/0.010
94MaMcSaWa (Majewski et al. 1994)				
011–000	5–14	67/67	1844–3643	0.014/0.050
020–011	1–10	27/27	1934–3024	0.013/0.050
022–000	2–8	9/11	4435–4795	0.017/0.030
022–011	1–10	57/63	1869–3293	0.013/0.040
022–100	5–6	1/2	2836–2836	0.010/0.010
031–011	n/a	0/1	nan–nan	nan/nan
031–020	1–7	2/2	2260–3002	0.010/0.010
033–011	3–4	2/2	4553–4721	0.020/0.030
033–022	3–7	3/4	2028–3241	0.010/0.010
100–000	7–11	4/4	3024–3277	0.010/0.010
111–000	6–7	1/1	4949–4949	0.040/0.040
111–011	1–9	13/18	2766–3288	0.067/0.707
111–100	2–11	36/38	1928–3204	0.011/0.042
120–022	6–7	1/1	3206–3206	0.010/0.010
122–020	9–10	1/1	2943–2943	0.010/0.010
122–022	n/a	0/1	nan–nan	nan/nan
94UyGaJaOk (Uy et al. 1994)				
011–000	1–16	73/73	2691–3579	0.011/0.040
100–000	8–10	2/2	3412–3441	0.010/0.010
94VeCaGuJo (Ventrudo et al. 1994)				
031 - 000	1–5	14/15	6807–7266	0.017/0.040
97DiNePoTe (Dinelli et al. 1997)				
000–020	n/a	0/1	nan–nan	nan/nan
011–000	6–14	14/16	2396–3269	0.012/0.040

Table 3 – *continued*

Vib.	J range	V/A	Energy range (cm^{-1})	Uncertainty Mean/Max (cm^{-1})
020–011	4–10	9/10	2622–2998	0.013/0.040
020–100	9–10	1/1	2893–2893	0.010/0.010
022–011	4–13	17/24	2413–3240	0.010/0.010
022–100	4–6	2/4	2571–2709	0.010/0.010
031–020	1–9	9/9	2458–2977	0.010/0.010
031–022	4–6	2/2	2680–2709	0.010/0.010
97DiNePoTe (Dinelli et al. 1997)				
033–022	0–9	19/20	2484–3061	0.010/0.010
100–000	8–8	1/1	2471–2471	0.010/0.010
111–011	4–7	5/9	2661–3203	0.020/0.030
111–100	4–11	7/7	2458–3294	0.013/0.030
120–022	2–6	2/2	2852–3052	0.010/0.010
120–111	4–6	2/2	2714–2817	0.025/0.040
122–111	2–7	7/7	2403–3022	0.010/0.010
211–200	1–6	3/3	2416–2654	0.010/0.010
00McOk (McCall & Oka 2000)				
120–000	3–4	1/1	8038–8038	0.010/0.010
122–000	1–5	27/27	7785–8163	0.014/0.040
211–000	4–6	2/2	8053–8123	0.010/0.010
01LiMc (Lindsay & McCall 2001)				
011–000	6–7	1/1	2956–2956	0.010/0.010
020–011	7–10	3/3	2902–2977	0.017/0.030
020–100	8–9	1/1	3003–3003	0.010/0.010
022–011	3–8	4/4	2601–2953	0.015/0.020
022–100	5–7	3/3	2844–2980	0.010/0.010
031–020	3–7	2/2	2596–2716	0.010/0.010
033–022	0–5	4/4	2469–2579	0.010/0.010
100–000	7–8	1/1	2957–2957	0.030/0.030
111–011	5–9	9/9	2437–3000	0.010/0.010
111–100	1–9	4/4	2575–2902	0.010/0.010
120–022	4–6	2/2	2976–2990	0.010/0.010
120–111	5–6	1/1	2817–2817	0.010/0.010
122–111	1–6	8/8	2497–2893	0.015/0.030
211–111	4–6	2/2	2891–2903	0.010/0.010
211–200	5–6	1/1	2654–2654	0.010/0.010
01LiMc_MAGIC (Lindsay & McCall 2001)				
000–000	0–1	3/3	22.839–86.960	1.00×10^{-9}/1.00×10^{-9}
01LiRaOk (Lindsay et al. 2001)				
011–000	4–16	96/96	3008–3596	0.008/0.045
020–011	8–13	6/6	2998–3283	0.007/0.015
020–100	9–10	1/1	3111–3111	0.010/0.010
022–011	4–12	75/75	3007–3527	0.007/0.040
022–100	7–9	4/4	3101–3269	0.013/0.035
031–020	5–8	2/2	3003–3134	0.005/0.005
033–022	5–6	1/1	3076–3076	0.010/0.010
100–000	4–11	22/22	3024–3575	0.009/0.045
111–011	0–9	24/25	3009–3443	0.006/0.015
111–100	6–10	14/14	3024–3296	0.006/0.010
120–020	6–7	1/1	3063–3063	0.015/0.015
120–022	5–6	2/2	3018–3052	0.005/0.005
122–020	5–5	1/1	3183–3183	0.005/0.005
122–111	6–7	2/2	3022–3236	0.005/0.005
200–100	6–8	3/3	3077–3104	0.008/0.010
03GoMcOk (Gottfried, McCall & Oka 2003)				
051–000	1–4	7/7	11019–11576	0.011/0.015
053–000	1–3	2/2	11044–11247	0.010/0.010
055–000	1–3	5/5	11572–11854	0.010/0.010
062–000	1–1	1/1	12419–12419	0.010/0.010
142–000	1–2	1/1	12246–12246	0.020/0.020
231–000	1–3	3/3	12222–12254	0.013/0.020
311–000	1–3	3/3	11112–11504	0.010/0.010
04MiKrWePl (Mikosch et al. 2004)				
031–000	1–3	3/3	7193–7241	0.015/0.026

Table 3 – *continued*

Vib.	J range	V/A	Energy range (cm^{-1})	Uncertainty Mean/Max (cm^{-1})
04OkEp (Oka & Epp 2004)				
011–000	1–7	20/20	2530–3182	0.011/0.020
022–000	1–7	10/11	4777–4987	0.015/0.054
04OkEp_CD (Oka & Epp 2004)				
000–000	1–10	68/69	7.255–1696	0.011/0.022
08KrBiRePe (Kreckel et al. 2008)				
051–000	1–2	2/2	11229–11244	0.010/0.010
055–000	0–2	4/4	11594–11882	0.010/0.010
062–000	1–2	5/5	12419–13072	0.011/0.014
142–000	1–2	2/2	12019–12087	0.010/0.010
144–000	1–2	1/1	12898–12898	0.010/0.010
231–000	0–1	1/1	12239–12239	0.010/0.010
311–000	0–2	4/4	11259–11511	0.010/0.010
322–000	1–2	1/1	13333–13333	0.010/0.010
08VeLeAgBe (Velilla et al. 2008)				
051–000	1–3	4/4	10730–10790	0.010/0.010
062–000	1–3	2/2	12503–13056	0.010/0.010
142–000	3–4	1/1	12658–12658	0.010/0.010
144–000	1–2	1/1	12898–12898	0.010/0.010
222–000	1–3	4/4	10726–10779	0.010/0.010
09MoGoOk (Morong et al. 2009)				
042–000	6–7	1/1	10329–10329	0.010/0.010
044–000	2–5	4/4	10367–10574	0.010/0.010
051–000	0–7	38/39	10462–11619	0.010/0.015
053–000	1–5	9/9	10657–11954	0.010/0.010
055–000	1–6	19/19	11331–12321	0.010/0.010
060–000	3–3	1/1	12116–12116	0.010/0.010
060–011	2–3	1/1	10828–10828	0.010/0.010
062–000	1–3	4/4	12419–13056	0.014/0.025
064–000	1–1	1/1	13597–13597	0.010/0.010
071–000	1–1	1/1	13676–13676	0.010/0.010
140–000	3–5	3/3	11563–12331	0.010/0.010
142–000	1–4	5/5	12102–12658	0.010/0.010
144–000	1–2	1/1	12898–12898	0.010/0.010
153–011	2–3	1/1	11265–11265	0.010/0.010
220–000	4–5	1/1	11114–11114	0.010/0.010
222–000	0–6	32/33	10322 –11115	0.010/0.010
231–000	1–6	7/7	11947 –12525	0.011/0.020
311–000	1–6	11/11	10875 –11892	0.010/0.010
12BeWoPe (Berg et al. 2012)				
144–000	1–2	1/1	12882–12882	0.005/0.005
231–000	1–2	1/1	12589–12589	0.005/0.005
233–000	1–2	1/1	12620–12620	0.005/0.005
12CrHoSiPe (Crabtree et al. 2012)				
011–000	1 - 2	1/1	2726–2726	0.004/0.004
12PaAdAlZo (Pavanello et al. 2012a)				
051–000	0–1	2/2	10799–10832	0.005/0.005
062–000	0–1	1/1	12413–12413	0.010/0.010
071–000	0–1	1/1	13638–13638	0.005/0.005
082–000	0–1	1/1	15059–15059	0.005/0.005
162–000	1–2	2/2	15130–15450	0.005/0.005
164–000	1–2	1/1	15643–15643	0.005/0.005
222–000	1–2	1/1	10752–10752	0.005/0.005
231–000	1–2	3/3	12374–12589	0.008/0.010
233–000	1–2	1/1	12620–12620	0.005/0.005
251–000	1–1	1/1	15717–15717	0.005/0.005
342–000	1–2	1/1	16506–16506	0.005/0.005
13HoPeJeSi (Hodges et al. 2013)				
011–000	1–5	10/10	2691–2894	2.40×10^{-5}/4.51×10^{-5}
13WuLiLiSh (Wu et al. 2013)				
011–000	1–4	12/12	2518–2918	3.14×10^{-4}/1.00×10^{-3}
15PeHoMaKo (Perry et al. 2015)				
011–000	3–7	10/10	2895–3030	6.93×10^{-5}/1.30×10^{-4}

Table 3 – *continued*

Vib.	J range	V/A	Energy range (cm^{-1})	Uncertainty Mean/Max (cm^{-1})
16JuKoScAs (Jusko et al. 2016)				
011–000	1–3	5/5	2691–2823	1.08×10^{-5}/2.20×10^{-5}
18GuChLiPe (Guan et al. 2018)				
011–000	1–6	16/16	2530–3015	5.20×10^{-5}/3.00×10^{-4}
19MaMc (Markus & McCall 2019)				
011–000	0–6	36/36	2217–3008	1.67×10^{-4}/6.33×10^{-4}
022–000	1–4	7/7	4968–5094	2.16×10^{-4}/6.45×10^{-4}
022–011	0–5	15/15	2474–2945	1.48×10^{-4}/2.16×10^{-4}

Table 4. The components of the updated H_2D^+ MARVEL network. The network is broken down by the transition data sources and the vibrational bands contained within them, given in the form ν_1', ν_2', ν_3' - ν_1'', ν_2'', ν_3''. For each band, the transition energy and total angular momentum J ranges are provided, along with the mean and maximum uncertainties for these transitions. The total number of transitions validated and accessed by MARVEL (V/A) are also provided.

Vib.	J range	V/A	Energy range (cm^{-1})	Uncertainty Mean/Max (cm^{-1})
84AmWa (Amano & Watson 1984)				
100–000	0–5	26/27	2841–3179	0.002/0.004
84BoDeDeDe (Bogey et al. 1984)				
000–000	1–1	1/1	12.423–12.423	6.67×10^{-6}/6.67×10^{-6}
84WaCoPeWo (Warner et al. 1984)				
000–000	1–1	1/1	12.423–12.423	3.34×10^{-6}/3.34×10^{-6}
85Amano (Amano 1985)				
100–000	0–5	37/37	2839–3208	0.006/0.040
85SaKaHi (Saito, Kawaguchi & Hirota 1985)				
000–000	2–2	1/1	5.2032–5.2032	1.23×10^{-6}/1.23×10^{-6}
86FoMcPeWa (Foster et al. 1986a)				
001–000	0–5	42/42	2109–2602	0.006/0.042
010–000	0–7	31/31	1838–2537	0.004/0.005
02FaDaKo (Farnik et al. 2002)				
002–000	1–2	1/1	4538–4538	0.002/0.002
011–000	0–2	3/3	4423–4513	8.67×10^{-4}/0.001
020–000	1–2	4/4	4271–4394	0.001/0.002
05AmHi (Amano & Hirao 2005)				
000–000	1–3	2/3	12.423–21.563	1.31×10^{-6}/1.67×10^{-6}
06Amano (Amano 2006)				
000–000	1–3	3/3	85.9513–115	2.72×10^{-5}/3.34×10^{-5}
06Amano_MAGIC (Amano 2006)				
000–000	0–1	1/1	60.030–60.030	1.00×10^{-5}/1.00×10^{-5}
06HlKoPlKo (Hlavenka et al. 2006a)				
021–000	0–2	3/3	6459–6491	0.021/0.031
07AsHuMuKu (Asvany et al. 2007)				
021–000	0–3	9/9	6341–6589	0.002/0.002
030–000	0–1	4/4	6242–6331	0.002/0.002
100–000	0–2	5/5	2947–3164	0.004/0.005
120–000	0–2	7/7	6946–7106	0.002/0.002
08AsRiMuWi (Asvany et al. 2008)				
000–000	0–1	1/1	45.701–45.701	6.67×10^{-7}/6.67×10^{-7}
09YoMaMoTa (Yonezu et al. 2009)				
000–000	0–3	8/8	5.2032–115	3.27×10^{-5}/2.01×10^{-4}
16JuKoScAs (Jusko et al. 2016)				
100–000	0–2	11/11	2887–3095	2.66×10^{-5}/1.50×10^{-4}
16JuKoScAs_CD (Jusko et al. 2016)				
000–000	0–2	4/4	66.4066–132	6.75×10^{-5}/1.51×10^{-4}
17JuToMuGh (Jusko et al. 2017)				
000–000	0–2	3/3	12.423–45.701	1.19×10^{-6}/3.07×10^{-6}

Table 5. The components of the updated D_2H^+ MARVEL network. The network is broken down by the transition data sources and the vibrational bands contained within them, given in the form ν_1', ν_2', ν_3' - $\nu_1'', \nu_2'', \nu_3''$. For each band, the transition energy and total angular momentum J ranges are provided, along with the mean and maximum uncertainties for these transitions. The total number of transitions validated and accessed by MARVEL (V/A) are also provided.

Vib.	J range	V/A	Energy range (cm^{-1})	Uncertainty Mean/Max (cm^{-1})
84LuAm (Lubic & Amano 1984)				
100–000	0–6	34/34	2638–2990	0.005/0.005
86FoMcWa (Foster, McKellar & Watson 1986b)				
001–000	0–5	35/35	1916–2291	0.005/0.005
010–000	0–6	53/53	1782–2280	0.004/0.005
90PoMc (Polyansky & McKellar 1990)				
010–000	3–4	1/1	2276–2276	0.005/0.005
02FaDaKoPo (Farnik et al. 2002)				
002–000	0–2	6/6	3994–4066	6.17×10^{-4}/9.00×10^{-4}
011–000	0–2	6/6	3983–4122	0.002/0.004
020–000	0–2	4/4	3847–3887	0.003/0.004
03HiAm (Hirao & Amano 2003)				
000–000	1–1	1/1	23.071–23.071	6.00×10^{-7}/6.00×10^{-7}
05AmHi (Amano & Hirao 2005)				
000–000	0–2	3/3	23.071–49.254	1.00×10^{-5}/1.00×10^{-5}
06HlPlBa (Hlavenka et al. 2006b)				
102–000	0–3	3/3	6534–6536	0.005/0.005
07AsHuMuKu (Asvany et al. 2007)				
102–000	0–2	5/5	6467–6536	0.005/0.005
111–000	0–1	1/1	6581–6581	0.005/0.005
120–000	0–1	1/1	6482–6482	0.005/0.005
08AsRiMuWi (Asvany et al. 2008)				
000–000	0–1	1/1	49.254–49.254	5.00×10^{-7}/5.00×10^{-7}
16JuKoScAs (Jusko et al. 2016)				
100–000	0–2	10/10	2684–2866	8.80×10^{-6}/2.60×10^{-5}
17JuToMuGh (Jusko et al. 2017)				
000–000	0–2	3/3	23.071–49.254	2.08×10^{-7}/3.34×10^{-7}
17YuPeAmMa (Yu. et al. 2017)				
000–000	1–3	5/5	34.646–98.311	3.34×10^{-6}/3.34×10^{-6}
17YuPeAmMa_MAGIC (Yu. et al. 2017)				
000–000	0–1	1/1	34.918–34.918	1.00×10^{-5}/1.00×10^{-5}
19MaKoMc (Markus et al. 2019)				
100–000	0–5	37/37	2588–2928	6.83×10^{-5}/1.15×10^{-4}

18GuChLiPe (Guan et al. 2018): Transition frequencies for 12 R-branch and 4 Q-branch transitions in the ν_2 band are presented. The majority are reported with sub-MHz accuracy. All of the transitions in this source had also been observed in other experiments (Lindsay & McCall 2001; Hodges et al. 2013; Perry et al. 2015; Jusko et al. 2016; Perry et al. 2016).

19MaMc (Markus & McCall 2019): The largest of the new H_3^+ data sources, providing 36 measurements of transitions in the $\nu_2 \leftarrow 0$ band, 15 transitions in the $2\nu_2^2 \leftarrow \nu_2$ band, and 7 transitions in the $2\nu_2^2 \leftarrow 0$ band. The data comprise a selection of P-, Q-, and R-branch transitions with uncertainties of 4 MHz. All of the reported transitions had been observed in prior studies (Watson et al. 1984; Majewski et al. 1987; Bawendi, Rehfuss & Oka 1990; Xu, Gabrys & Oka 1990; Uy et al. 1994; McKellar & Watson 1998; Guan et al. 2018; Markus et al. 2018).

In total there were 102 new transitions to be added to the existing set of 1610 transitions and a further 7 transitions that had been missed in the original MARVEL compilation. The inclusion of the new transitions allowed us to validate 19 previously invalidated transitions. 7 transitions had their assignment corrected based on updated assignments provided in subsequent papers. A further 9 transitions were reassigned based on apparent mixing identified through comparison with the empirical MARVEL energies. 2 transition assignments were updated based on suggestions provided by Jaquet (2022). Sarka & Poirier (2022) provided a series of assignments for H_3^+ which were used to correct the assignments of 41 transitions and to assign 22 previously unassigned transitions. A further three unassigned transitions from the literature were assigned based on comparison with the MARVEL energy levels. The new transition assignments are detailed in Table 2. The transitions updated in this way all involve levels with relatively high energies in a region where accurate determination of the vibrational state can be challenging. In total, 59 transitions from the original network were reassigned and an additional 8 had their assignment corrected due to digitization errors from the original source.

Table 6. The assigned vibrational bands of the D_3^+ states file, detailing the J range and maximum energy of each band.

ν_1	ν_2	L_2	Count	Energy range (cm^{-1})	J range
0	0	0	256	0–4753	0–15
0	1	1	380	1835–6300	0–15
0	2	0	99	3531–6830	0–15
0	2	2	253	3646–7551	0–15
0	3	1	11	5214–5513	0–3
0	3	3	6	5401–5513	0–1
0	4	0	1	6774	0
0	4	2	2	6860–6860	0
0	4	4	2	7170–7170	0
0	5	1	2	8298–8298	0
0	5	3	2	8376–8600	0
0	5	5	2	8791–8791	0
0	6	0	1	9696	0
0	6	2	2	9731–9731	0
1	0	0	140	2301–5436	0–15
1	1	1	99	4060–7800	0–14
1	2	0	4	5712–5756	0–1
1	2	2	4	5796–6169	0–4
1	3	1	2	7368–7368	0
1	3	3	2	7454–7536	0
1	4	0	1	8864	0
1	4	2	2	9031–9031	0
1	4	4	2	9163–9163	0
2	0	0	36	4555–5178	0–5
2	1	1	2	6237–6237	0
2	2	0	1	7831	0
2	2	2	2	7894–7894	0
2	3	1	2	9424–9424	0
2	3	3	2	9463–9555	0
3	0	0	1	6761	0
3	1	1	2	8366–8366	0
3	2	0	1	9896	0
3	2	2	2	9943–9943	0
4	0	0	1	8921	0

The final set of 1719 transitions were passed through MARVEL for validation, with 1656 being validated; these transitions are summarized in Table 3. The network is divided into 39 components, the largest of which comprises 1580 transitions which determine 703 empirical energy levels. Of the remaining components: two consist of 6 transitions; one of 5 transitions; two of 4 transitions; three of 3 transitions; 12 of 2 transitions and the remaining 18 of single transitions. As these minor components are not connected to the primary component, the energies of the levels within them are not determined relative to the zero-energy level and are hence not considered further.

Table 7. Statistics for the new line lists, detailing: the maximum J value for each; the maximum temperature up to which the line list is complete; the maximum lower state energy involved in a transition; the maximum upper state energy involved in a transition; the total number of transitions and the total number of transitions between MARVELized states.

Species	J_{max}	T_{max} (K)	E_{low} (cm^{-1})	E_{high} (cm^{-1})	No. trans	No. MARVELized trans
H_3^+	37	5000	25 189.709 34	42 000.743 57	127542657	17147
H_2D^+	20	1750	6988.914 26	18 496.216 69	22164810	895
D_2H^+	25	2000	8253.939 824	34 838.528 613	2290235000	905
D_3^+	15	800	2639.965 597	17 234.642 274	36078183	0

Table 8. Excerpts from the H_3^+ and D_3^+ states files, using the format defined by Tennyson et al. (2013). Note that the zero-energy level of H_3^+ with A_1' symmetry does not exist and hence has 'nan' entries for its lifetime and isomer. Any row for which the ν_1, ν_2, L_2, G, U, or K assignment is not known will likewise have 'nan' entries in these columns.

i	$\tilde{E}$	g_{tot}	J	unc	τ	e/f	Γ_{rve}	No.	Isomer	ν_1	ν_2	L_2	G	U	K	Source tag
							H_3^+									
1	0.000 000	0	0	0.000 000	nan	e	A1'	1	nan	0	0	0	0	m	0	Ma
2	2521.410 484	2	0	0.000 133	8.4474e−03	e	E'	1	p	0	1	1	1	m	0	Ma
3	4998.052 947	2	0	0.010 004	2.4871e−03	e	E'	2	p	0	2	2	2	m	0	Ma
4	5554.061 000	2	0	0.010 000	7.3144e−03	e	E'	3	p	1	1	1	1	m	0	Ca
5	7005.974 780	2	0	0.010 000	3.1660e−03	e	E'	4	p	0	3	1	1	m	0	Ca
6	7870.229 810	2	0	0.010 000	2.5047e−03	e	E'	5	p	1	2	2	2	m	0	Ca
7	8488.013 160	2	0	0.010 000	6.6336e−03	e	E'	6	p	2	1	1	1	m	0	Ca
8	9113.041 390	2	0	0.010 000	2.0836e−03	e	E'	7	p	0	4	2	2	m	0	Ca
9	9653.699 850	2	0	0.010 000	1.1122e−03	e	E'	8	p	1	3	1	1	m	0	Ca
10	9997.183 130	2	0	0.010 000	1.0631e−03	e	E'	9	p	0	4	4	4	m	0	Ca
							D_3^+									
1	0.0000 000	10	0	0.0000 000	inf	+	A1'	1	o	0	0	0	0	m	0	EH
2	2301.1985 530	10	0	0.1000 000	9.6693e+00	+	A1'	2	o	1	0	0	0	m	0	Ca
3	3530.6654 530	10	0	0.1000 000	2.4171e−02	+	A1'	3	o	0	2	0	0	m	0	Ca
4	4554.7949 320	10	0	0.1000 000	3.2217e+00	+	A1'	4	o	2	0	0	0	m	0	Ca
5	5400.9592 930	10	0	0.1000 000	6.7375e−03	+	A1'	5	o	0	3	3	3	m	0	Ca
6	5711.9821 150	10	0	0.1000 000	1.4546e−02	+	A1'	6	o	1	2	0	0	m	0	Ca
7	6761.1836 300	10	0	0.1000 000	1.3900e+00	+	A1'	7	o	3	0	0	0	m	0	Ca
8	6774.1319 250	10	0	0.1000 000	8.2880e−03	+	A1'	8	o	0	4	0	0	m	0	Ca
9	7453.9598 120	10	0	0.1000 000	7.3275e−03	+	A1'	9	o	1	3	3	3	m	0	Ca
10	8375.5588 740	10	0	0.1000 000	6.3728e−03	+	A1'	10	o	0	5	3	3	m	0	Ca

Notes. i: State counting number;
$\tilde{E}$: Term value (in cm^{-1});
g_{tot}: Total state degeneracy;
J: Total angular momentum quantum number;
unc: Estimated uncertainty of energy level (in cm^{-1});
τ: Radiative lifetime (in seconds);
e/f: Rotationless parity;
Γ_{rve}: D_{3h} symmetry group;
No.: Symmetry group block counting number;
Isomer: Nuclear spin isomer;
ν_1: Symmetric stretching quantum number;
ν_2: Bending quantum number;
L_2: Vibrational angular momentum quantum number;
G: Absolute value of $k - l_2$;
U: U-notation of Watson (1994);
K: Rotational angular momentum quantum number;
Source Tag: The method used to generate the term value; 'Ma' for MARVELized energies, 'EH' for energies from effective Hamiltonian calculations and 'Ca' for energies calculated using DVR3D.

2.1.2 H_2D^+ network

A MARVEL network for H_2D^+ was originally produced by Furtenbacher et al. (2013b) and contained transition data from 13 sources. Since then, two new sets of transition measurements have been published by Jusko et al. (2016, 2017).

16JuKoScAs (Jusko et al. 2016): Transitions frequencies for 11 ν_1 band transitions are reported with MHz and sub-MHz accuracy. This source provides significantly higher accuracy measurements of transitions previously observed by Amano (1985).

17JuToMuGh (Jusko et al. 2017): 3 pure-rotation transition measurements are provided with sub-MHz or kHz accuracy.

Table 9. Excerpts from the H_2D^+ and D_2H^+ states files, using the format defined by Tennyson et al. (2013). Any row for which the ν_1, ν_2, ν_3, K_a, or K_c assignment is not known will have 'nan' entries in these columns.

i	$\tilde{E}$	g_{tot}	J	unc	τ	+/−	Γ_{rve}	No.	Isomer	ν_1	ν_2	ν_3	K_a	K_c	Source tag
							H_2D^+								
1	0.0000 000	3	0	0.0000 000	inf	+	A1	1	p	0	0	0	0	0	Ma
2	2205.8771 127	3	0	0.0050 000	5.7143e−02	+	A1	2	p	0	1	0	0	0	Ma
3	2992.5022 357	3	0	0.0000 050	1.8706e−02	+	A1	3	p	1	0	0	0	0	Ma
4	4287.4732 000	3	0	0.2000 000	1.8812e−02	+	A1	4	p	0	2	0	0	0	Ca
5	4602.6196 400	3	0	0.2000 000	3.1868e−03	+	A1	5	p	0	0	2	0	0	Ca
6	5039.7666 100	3	0	0.2000 000	1.9520e−02	+	A1	6	p	1	1	0	0	0	Ca
7	5877.2574 100	3	0	0.2000 000	1.0870e−02	+	A1	7	p	2	0	0	0	0	Ca
8	6287.6671 127	3	0	0.0020 000	6.4627e−03	+	A1	8	p	0	3	0	0	0	Ma
9	6645.7008 700	3	0	0.3000 000	2.5443e−03	+	A1	9	p	0	1	2	0	0	Ca
10	6991.5781 127	3	0	0.0020 000	9.4938e−03	+	A1	10	p	1	2	0	0	0	Ma
							D_2H^+								
1	0.0000 000	12	0	0.0000 000	inf	+	A1	1	o	0	0	0	0	0	Ma
2	1968.1622 648	12	0	0.0050 000	1.9317e−02	+	A1	2	o	0	1	0	0	0	Ma
3	2736.9754 969	12	0	0.0000 040	1.1633e−02	+	A1	3	o	1	0	0	0	0	Ma
4	3821.2081 670	12	0	0.1000 000	1.2227e−02	+	A1	4	o	nan	nan	nan	nan	nan	Ca
5	4042.7721 648	12	0	0.0009 000	1.2305e−02	+	A1	5	o	0	0	2	0	0	Ma
6	4648.7587 400	12	0	0.2000 000	6.4298e−03	+	A1	6	o	nan	nan	nan	nan	nan	Ca
7	5385.3522 270	12	0	0.2000 000	6.0840e−03	+	A1	7	o	nan	nan	nan	nan	nan	Ca
8	5579.1928 220	12	0	0.2000 000	8.0766e−03	+	A1	8	o	nan	nan	nan	nan	nan	Ca
9	6008.5163 100	12	0	0.3000 000	4.8418e−03	+	A1	9	o	nan	nan	nan	nan	nan	Ca
10	6432.5596 700	12	0	0.3000 000	6.6492e−03	+	A1	10	o	nan	nan	nan	nan	nan	Ca

Notes. i: State counting number;
$\tilde{E}$: Term value (in cm^{-1});
g_{tot}: Total state degeneracy;
J: Total angular momentum quantum number;
unc: Estimated uncertainty of energy level (in cm^{-1});
τ: Radiative lifetime (in seconds);
+/-: Total parity;
Γ_{rve}: C_{2v} symmetry group;
No.: Symmetry group block counting number;
Isomer: Nuclear spin isomer;
ν_1: Symmetric stretching quantum number;
ν_2: Bending quantum number;
ν_3: Asymmetrical stretching quantum number;
K_a: Rotational angular momentum quantum number;
K_c: Rotational angular momentum quantum number;
Source Tag: The method used to generate the term value; 'Ma' for MARVELized energies, 'EH' for energies from effective Hamiltonian calculations and 'Ca' for energies calculated using DVR3D.

Table 10. Excerpts from the trans files for the new line lists for D_2H^+ and D_3^+.

D_2H^+			D_3^+		
f	i	A_{fi} (s^{-1})	f	i	A_{fi} (s^{-1})
1401	1	3.30142477E−03	226	16	5.65667085E−09
1402	2	2.19499998E−03	229	16	2.93922054E−02
3	1402	1.59575873E−01	216	226	1.30736782E−07
1403	2	1.80478736E−03	1023	226	4.95756630E−07
3	1403	4.59507405E−02	1025	226	5.90452177E−07
1404	2	9.63358275E−02	1028	226	6.58440901E−02
1404	3	3.99647847E−03	2	212	1.03419866E−01
1405	4	2.49561352E−03	1013	212	2.22162053E−02
5	1405	2.09336332E−03	229	216	3.39285830E−02
6	1405	3.28445005E−01	1043	216	4.03805710E−07

Notes. f: The upper state counting number from the corresponding states file.
i: The lower state counting number from the corresponding states file.
A_{fi}: The Einstein A coefficient.

These two new sources and a 'magic' forbidden transition to connect the nuclear spin isomers, derived from effective Hamiltonian calculations using molecular constants from Amano (2006), brought the total number of transitions for H_2D^+ to 210; these are summarized in Table 4. 208 transitions were validated successfully by MARVEL, yielding a final network comprising 7 components, the largest of which contained 200 transitions that determine 109 unique energy levels. For the remaining 6 components, one contained 3 transitions while the rest are single transition components; these disconnected components are not considered further here.

2.1.3 D_2H^+ network

The D_2H^+ MARVEL network was originally published by Furtenbacher et al. (2013b) and was constructed using transition data from 9 sources. Four new sets of transition data have subsequently been published (Jusko et al. 2016, 2017; Yu. et al. 2017; Markus, Kocheril & McCall 2019) and have now been added to the existing network.

Table 11. Adjusted nuclear spin statistical weights for the levels of D_3^+ for which C_{2v} symmetries are used.

Γ_{rve}	g_{ns}
A_1, A_2	6
B_1, B_2	3

Table 12. The partition functions for each new line list, calculated for a range of temperatures up to each line list's maximum temperature, given in Table 7.

Temp. (K)	H_3^+	H_2D^+	D_2H^+	D_3^+
10	6.0000×10^{-4}	3.0181×10^{0}	1.2153×10^{1}	1.0235×10^{1}
50	2.0215×10^{0}	1.5141×10^{1}	3.7355×10^{1}	2.7175×10^{1}
100	7.3972×10^{0}	4.5354×10^{1}	9.7278×10^{1}	6.9095×10^{1}
200	2.0733×10^{1}	1.2604×10^{2}	2.6721×10^{2}	1.9085×10^{2}
300	3.7609×10^{1}	2.2937×10^{2}	4.8756×10^{2}	3.4904×10^{2}
400	5.7650×10^{1}	3.5231×10^{2}	7.5053×10^{2}	5.3858×10^{2}
500	8.0581×10^{1}	4.9357×10^{2}	1.0549×10^{3}	7.6022×10^{2}
600	1.0640×10^{2}	6.5391×10^{2}	1.4048×10^{3}	1.0188×10^{3}
700	1.3533×10^{2}	8.3572×10^{2}	1.8080×10^{3}	1.3215×10^{3}
800	1.6783×10^{2}	1.0426×10^{3}	2.2746×10^{3}	1.6761×10^{3}
900	2.0442×10^{2}	1.2787×10^{3}	2.8162×10^{3}	
1000	2.4578×10^{2}	1.5489×10^{3}	3.4456×10^{3}	
1250	3.7478×10^{2}	2.4087×10^{3}	5.4967×10^{3}	
1500	5.5089×10^{2}	3.6069×10^{3}	8.4351×10^{3}	
1750	7.8938×10^{2}	5.2510×10^{3}	1.2563×10^{4}	
2000	1.1086×10^{3}		1.8242×10^{4}	
3000	3.7032×10^{3}			
4000	1.0239×10^{4}			
5000	2.4177×10^{4}			

16JuKoScAs (Jusko et al. 2016): This source provides 10 transitions frequencies observed with sub-MHz accuracy. 8 of these transitions had been previously observed by Lubic & Amano (1984).

17JuToMuGh (Jusko et al. 2017): 3 ground state pure-rotation transition measurements are provided with kHz accuracy.

17YuPeAmMa (Yu. et al. 2017): This source reports 5 ground state pure-rotation transitions with sub-MHz accuracy. 4 of these transitions had not been reported in other sources, with the other also being observed by Jusko et al. (2017).

19MaKoMc (Markus et al. 2019): Transition frequencies for 37 ν_1 band transitions are provided with MHz accuracy. 10 of the transitions in this source are new and had not been reported elsewhere, while the rest had been observed by Lubic & Amano (1984) and Jusko et al. (2016).

With the addition of 55 new transition measurements, the new network contains 210 transitions. Two existing transitions that had digitization errors in their transition frequencies were updated to the correct values. A 'magic' forbidden transition is included to connect the otherwise distinct ortho and para components of the network, using a frequency calculated by Yu. et al. (2017). The final set of D_2H^+ transition data is summarized in Table 5. All of the transitions in the network were validated by MARVEL, yielding a primary network component containing 200 transitions which define 115 unique energy levels. The rest of the transitions are present in 7 disconnected components, one of which contains 3 transitions, another 2 transitions and the remainder are single transition components.

2.2 Effective Hamiltonians

There have been significantly fewer observations of D_3^+ spectra than of the three other isotopologues considered here. As such, there was insufficient data to build a well-connected network. In lieu of this, we used effective Hamiltonian constants from Watson et al. (1987) and Amano et al. (1994) to calculate energies for the states in the range $J = 0 - 15$, up to a maximum energy of 2676.387 cm^{-1}. These calculations were performed using the program PGOPHER (Western 2017) which also provides full state assignments for the levels it computes. Hence, full quantum number assignments were determined via this method for 282 levels within the bands for which constants were available: 188 levels in the 000 band (ν_1, ν_2, L_2); 2 levels in the 010 band; 105 in the 011 band; 22 in the 100 band. The majority of the levels assigned through this method have $J < 10$. Further assignments were done manually for states at higher energies with the aid of the vibrational band origins published by Amano et al. (1994) and the assigned hot and overtone bands published by Alijah, Wolniewicz & Hinze (1995). A further 1045 states were assigned this way and a breakdown of the assigned bands is given in Table 6. These assignments were added to the calculated states file, given that DVR3D only provides assignments for the rigorous quantum numbers: J, rotationless parity *e/f* and interchange of two of the D atoms.

3 LINE LIST CALCULATIONS

3.1 Updated H_3^+ and H_2D^+

While the main line lists were computed using DVR3D, we took advantage of calculations by Sarka, Das & Poirier (2021), Sarka & Poirier (2022) performed using the variational nuclear motion programs SCALIT (Chen & Poirier 2006a, b, 2010a, b; Petty & Poirier 2014), and GENIUSH (Mátyus, Czakó & Császár 2009; Fábri, Mátyus & Császár 2011) to give full quantum number designations. The approach applied is detailed by Sarka & Poirier (2022) but we provide a quick summary of the main steps here. First, using Jacobi coordinates SCALIT calculations were carried out in the four blocks of the G_4 permutation–inversion (PI) symmetry group. Due to the very high convergence accuracy, the full G_{12} PI group labels (Γ_{rve}) were easily assigned unambiguously using the $\Gamma(G_{12}/D_{3h})\downarrow G_4$ correlation table. Next, calculations were repeated with the code GENIUSH with slightly lower accuracy, but still sufficient to match the energy levels with the SCALIT ones. After the vibrational states were labelled (ν_1, ν_2, L_2), vibrational parent labels were semi-automatically assigned to rovibrational states using the rigid rotor decomposition scheme (RRD) implemented in GENIUSH (Mátyus et al. 2010). The RRD overlaps of GENIUSH also help to assign the rotational quantum numbers (J, G, U, K), as the symmetric top rigid rotor functions are labelled by K. Using this method, we were able to label by the quantum number set (ν_1, ν_2, L_2, J, G, U, K, Γ_{rve}), an additional 1525 states in the MiZATeP H_3^+ line list.

The energies of the existing H_3^+ and H_2D^+ line lists were updated with empirical energies where they were known. For levels with matching assignments in both the states files and corresponding MARVEL network, the term energies and their uncertainties were set to the values determined by the MARVEL procedure. For the levels that did not exist within the molecules' MARVEL network, the calculated term energies were retained and estimates for their uncertainties were calculated as follows

$$\Delta\tilde{E} = \begin{cases} 0.1, & \text{if } \tilde{E} < 2000 \\ \lfloor \tilde{E}/2000 \rfloor / 10, & \text{otherwise.} \end{cases} \quad (2)$$

3.2 New line lists

New line lists were computed for D_2H^+ and D_3^+ molecular ions. Both calculations used the highly accurate global *ab initio* PES, together with adiabatic and relativistic correction surfaces, computed by

Table 13. Predicted pure-rotation transition wavenumbers and Einstein A coefficients for transitions involving low-energy lower levels for H_3^+ and D_3^+. For all upper and lower levels included here, $v_1 = v_2 = L_2 = 0$. Values quoted in brackets for energies are the uncertainty in the last digit.

		Upper level						Lower level					
Wavenumber (cm^{-1})	A_{fi} (s^{-1})	J	G	U	K	Γ_{rve}	Term energy (cm^{-1})	J	G	U	K	Γ_{rve}	Term energy (cm^{-1})
							H_3^+						
105.17639(37)	4.2570×10^{-7}	2	2	m	2	E'	169.297 39(37)	1	1	m	1	E''	64.121 000(0)
68.05481(37)	5.6141×10^{-7}	2	1	m	1	E''	237.352 195(50)	2	2	m	2	E'	169.297 39(37)
325.46535(40)	3.4982×10^{-5}	3	1	m	1	E''	494.762 74(14)	2	2	m	2	E'	169.297 39(37)
190.66548(40)	1.7422×10^{-5}	3	2	m	2	E'	428.017 68(39)	2	1	m	1	E''	237.352 195(50)
201.52843(29)	7.3590×10^{-5}	3	0	m	0	A_2'	516.880 36(23)	3	3	m	3	A_2''	315.351 92(18)
66.74506(42)	2.6423×10^{-6}	3	1	m	1	E''	494.762 74(14)	3	2	m	2	E'	428.017 68(39)
405.55623(42)	3.2067×10^{-4}	4	1	m	1	E''	833.573 91(14)	3	2	m	2	E'	428.017 68(39)
7.27431(27)	2.5602×10^{-9}	4	4	m	4	E'	502.037 05(23)	3	1	m	1	E''	494.762 74(14)
273.70656(44)	1.7953×10^{-4}	4	2	m	2	E'	768.469 30(42)	3	1	m	1	E''	494.762 74(14)
							D_3^+						
53.3000(28)	1.3067×10^{-8}	2	2	m	2	E'	85.6210(20)	1	1	m	1	E''	32.3210(20)
33.7470(28)	1.6552×10^{-8}	2	1	m	1	E''	119.3680(20)	2	2	m	2	E'	85.6210(20)
163.7280(28)	1.0739×10^{-6}	3	1	m	1	E''	249.3490(20)	2	2	m	2	E'	85.6210(20)
96.5440(28)	5.5135×10^{-7}	3	2	m	2	E'	215.9120(20)	2	1	m	1	E''	119.3680(20)
29.2810(28)	3.1041×10^{-8}	3	−3	m	3	A_1''	159.8680(20)	2	0	m	0	A_1'	130.5870(20)
100.5990(28)	2.1970×10^{-6}	3	0	m	0	A_2'	260.4660(20)	3	3	m	3	A_2''	159.8670(20)
272.6900(28)	1.4422×10^{-5}	4	0	m	0	A_1'	432.5580(20)	3	−3	m	3	A_1''	159.8680(20)
33.4370(28)	8.0083×10^{-8}	3	1	m	1	E''	249.3490(20)	3	2	m	2	E'	215.9120(20)
205.6600(28)	1.0260×10^{-5}	4	1	m	1	E''	421.5720(20)	3	2	m	2	E'	215.9120(20)
5.6660(28)	3.0205×10^{-10}	4	4	m	4	E'	255.0150(20)	3	1	m	1	E''	249.3490(20)
139.0820(28)	5.7366×10^{-6}	4	2	m	2	E'	388.4310(20)	3	1	m	1	E''	249.3490(20)

Pavanello et al. (2012a, b) which were used for the MiZATeP line list. To calculate transition intensities, the high-accuracy DMS obtained for the H_3^+ system was used (Petrignani et al. 2014). This DMS was obtained by fitting seven parameters to a polynomial form written in terms of effective charges (see Röhse et al. 1994). This DMS was centred on the centre-of-mass ensuring the correct treatment of the centre-of-charge – centre-of-mass displacement which leads to D_2H^+ (and H_2D^+) having a permanent dipole moment.

The DVR3D program suite (Tennyson et al. 2004) was used to compute the final line lists. As part of this project, a new module was added to this suite which converts DVR3D results to ExoMol format (Tennyson, Hill & Yurchenko 2013) comprising a states and trans file, and allowing spectra to be easily generated using EXOCROSS (Yurchenko, Al-Refaie & Tennyson 2018). The module reads the energy levels and Einstein coefficients from DVR3D, requiring as input from the user, the molecular symmetry, C_s or C_{2v}, and the nuclear statistic weight for each symmetry. The program, called LINELIST, is available as part of the DVR3D program suite from the ExoMol GitHub pages.

As with H_3^+ and H_2D^+, the calculated term energies of D_2H^+ were updated with empirical values from the new MARVEL network where available. Likewise, the unchanged calculated energies of the new D_2H^+ and D_3^+ line lists had uncertainties estimated using equation (2).

3.3 D_2H^+ nuclear motion calculations

DVR3D nuclear motion calculations were performed in the following way: with 31, 31, and 50 grid points for two radial and an angular scattering coordinates. The calculations used Morse-like oscillators with parameters 3.1, 0.1, and 0.006 for r_1 (D–D) radial coordinate, and spherical oscillators with parameters 0, 0, and 0.016 for the r_2 (H–D_2 scattering coordinate). The dimension of the final vibrational Hamiltonians were set to 5000. Calculations included all levels up to 15 000 cm^{-1} for $J \leq 25$. 1500 vibrational basis functions calculated using DVR3DRJZ were passed to ROTLEV3 for the rotational step of the calculation. Following Polyansky & Tennyson (1999), nuclear masses $m_H = 1.007276$ Da and $m_D = 2.013553$ Da were used for rotational motion and effective masses intermediate between nuclear and atomic masses $m_H = 1.007537$ Da and $m_D = 2.013814$ Da were used for the vibrational motion. This formulation has been shown to allow for non-adiabatic effects in the calculation. The resulting MiZo line list is complete up to a temperature of 2000 K.

3.4 D_3^+ nuclear motion calculations

DVR3D calculations for D_3^+ were performed using the same size grids and Hamiltonians as those specified for D_2H^+ above (31, 31, and 50 grid points for two radial and an angular scattering coordinates, correspondingly, and the final Hamiltonian dimensions equal to 5000). The calculations used Morse-like oscillators with parameters 2.6, 0.1, and 0.006 for the r_1 coordinate, and spherical oscillators with parameters 0, 0, and 0.016 for the r_2 coordinate. Nuclear masses equal to $m_D = 2.013553$ Da were used for all calculations.

On the basis of nuclear motion calculation results and the DMS by Petrignani et al. (2014) a linelist in the frequency region up to 15 000 cm^{-1} for a temperature of 800 K and using the corresponding partition function value 118.7 together with a list of corresponding energy levels for D_3^+ was computed. This linelist contains transitions between energy states with J values 0–15 and energies 0–15 500 cm^{-1}. The new MiZo D_3^+ line list is complete up to a temperature of 800 K.

Statistics for all of the line lists presented here are given in Table 7.

3.5 States files

New states files are provided for each of the four species considered here and are formatted using the standard outlined by Tennyson et al. (2013). H_3^+ and D_3^+ are identified using the same set of quantum numbers and hence their states files contain the same columns.

Table 14. Predicted pure-rotation transition wavenumbers and Einstein A coefficients for transitions involving low-energy lower levels for H_2D^+ and D_2H^+. For all upper and lower levels included here, $v_1 = v_2 = v_3 = 0$. Values quoted in brackets for the transition frequencies are the uncertainty in the last digit.

		Upper level					Lower level				
Wavenumber (cm^{-1})	A_{fi} (s^{-1})	J	K_a	K_c	Γ_{rve}	Term energy (cm^{-1})	J	K_a	K_c	Γ_{rve}	Term energy (cm^{-1})
						H_2D^+					
45.7011 127(4)	4.0400×10^{-3}	1	0	1	A_2	45.7011 127(4)	0	0	0	A_1	0.0000 000(0)
85.9513 50(33)	3.0300×10^{-2}	2	0	2	A_1	131.652 463(33)	1	0	1	A_2	45.7011 127(4)
178.1566(36)	1.6600×10^{-2}	2	2	0	A_1	223.8577(36)	1	0	1	A_2	45.7011 127(4)
12.422 639(14)	1.2200×10^{-4}	1	1	0	B_2	72.452 486(10)	1	1	1	B_1	60.029 846(10)
78.829 277(23)	1.8800×10^{-2}	2	1	2	B_2	138.859 124(21)	1	1	1	B_1	60.029 846(10)
103.482 549(23)	4.2400×10^{-2}	2	1	1	B_1	175.935 034(21)	1	1	0	B_2	72.452 486(10)
87.0021(36)	3.2700×10^{-3}	2	2	1	A_2	218.6545(36)	2	0	2	A_1	131.652 463(33)
119.7622(20)	8.5300×10^{-2}	3	0	3	A_2	251.4146(20)	2	0	2	A_1	131.652 463(33)
244.6884(70)	4.7600×10^{-2}	3	2	1	A_2	376.3409(70)	2	0	2	A_1	131.652 463(33)
37.075911(30)	1.0700×10^{-3}	2	1	1	B_1	175.935 034(21)	2	1	2	B_2	138.859 124(21)
115.201 469(33)	7.3200×10^{-2}	3	1	3	B_1	254.060 593(26)	2	1	2	B_2	138.859 124(21)
319.4843(70)	2.3600×10^{-2}	3	3	1	B_1	458.3434(70)	2	1	2	B_2	138.859 124(21)
150.2252(20)	1.5900×10^{-1}	3	1	2	B_2	326.1602(20)	2	1	1	B_1	175.935 034(21)
283.8945(70)	3.7500×10^{-2}	3	3	0	B_2	459.8296(70)	2	1	1	B_1	175.935 034(21)
5.2032(50)	1.1300×10^{-5}	2	2	0	A_1	223.8577(36)	2	2	1	A_2	218.6545(36)
136.1238(79)	7.7800×10^{-2}	3	2	2	A_1	354.7783(70)	2	2	1	A_2	218.6545(36)
27.5569(41)	9.5600×10^{-6}	3	0	3	A_2	251.4146(20)	2	2	0	A_1	223.8577(36)
152.4832(79)	1.1200×10^{-1}	3	2	1	A_2	376.3409(70)	2	2	0	A_1	223.8577(36)
103.3637(73)	8.2700×10^{-3}	3	2	2	A_1	354.7783(70)	3	0	3	A_2	251.4146(20)
151.38(10)	1.8100×10^{-1}	4	0	4	A_1	402.80(10)	3	0	3	A_2	251.4146(20)
329.972(10)	6.7000×10^{-2}	4	2	2	A_1	581.386(10)	3	0	3	A_2	251.4146(20)
527.62(10)	4.6500×10^{-3}	4	4	0	A_1	779.04(10)	3	0	3	A_2	251.4146(20)
72.0997(20)	4.1900×10^{-3}	3	1	2	B_2	326.1602(20)	3	1	3	B_1	254.060 593(26)
149.6189(53)	1.7400×10^{-1}	4	1	4	B_2	403.6795(53)	3	1	3	B_1	254.060 593(26)
205.7690(70)	3.1700×10^{-3}	3	3	0	B_2	459.8296(70)	3	1	3	B_1	254.060 593(26)
391.51(10)	5.2800×10^{-2}	4	3	2	B_2	645.57(10)	3	1	3	B_1	254.060 593(26)
						D_2H^+					
49.2542 648(2)	3.3014×10^{-3}	1	1	1	A_2	49.2542 648(2)	0	0	0	A_1	0.0000 000(0)
23.071 309(14)	5.0885×10^{-4}	1	1	0	B_2	57.989 629(10)	1	0	1	B_1	34.918 320(10)
75.341 734(30)	1.0592×10^{-2}	2	1	2	B_2	110.260 054(28)	1	0	1	B_1	34.918 320(10)
52.4637 522(33)	2.0691×10^{-3}	2	0	2	A_1	101.7180 170(33)	1	1	1	A_2	49.2542 648(2)
132.809 827(10)	4.4605×10^{-2}	2	2	0	A_1	182.064 091(10)	1	1	1	A_2	49.254 2648(2)
121.174 679(68)	4.4481×10^{-2}	2	2	1	B_1	179.164 308(67)	1	1	0	B_2	57.989 629(10)
34.6460 731(47)	1.2985×10^{-3}	2	1	1	A_2	136.3640 901(34)	2	0	2	A_1	101.7180 170(33)
98.3110 072(57)	2.4763×10^{-2}	3	1	3	A_2	200.0290 242(47)	2	0	2	A_1	101.7180 170(33)
68.9042 54(73)	4.5854×10^{-3}	2	2	1	B_1	179.164 308(67)	2	1	2	B_2	110.260 054(28)
85.8400 24(73)	1.4620×10^{-2}	3	0	3	B_1	196.100 078(67)	2	1	2	B_2	110.260 054(28)
185.781 201(73)	5.4468×10^{-2}	3	2	1	B_1	296.041 254(67)	2	1	2	B_2	110.260 054(28)
45.7000 01(11)	2.2792×10^{-3}	2	2	0	A_1	182.064 091(10)	2	1	1	A_2	136.3640 901(34)
146.951 256(94)	6.2260×10^{-2}	3	2	2	A_1	283.315 346(94)	2	1	1	A_2	136.3640 901(34)
72.137 151(95)	1.7139×10^{-3}	3	1	2	B_2	251.301 459(67)	2	2	1	B_1	179.164 308(67)
17.964 933(11)	5.6565×10^{-6}	3	1	3	A_2	200.0290 242(47)	2	2	0	A_1	182.064 091(10)
55.201 381(95)	3.5511×10^{-3}	3	1	2	B_2	251.301 459(67)	3	0	3	B_1	196.100 078(67)
121.1511(50)	5.0954×10^{-2}	4	1	4	B_2	317.2512(50)	3	0	3	B_1	196.100 078(67)
83.286 322(94)	8.5394×10^{-3}	3	2	2	A_1	283.315 346(94)	3	1	3	A_2	200.0290 242(47)
115.707 967(94)	4.3474×10^{-2}	4	0	4	A_1	315.736 992(94)	3	1	3	A_2	200.0290 242(47)
44.739 796(95)	2.9105×10^{-3}	3	2	1	B_1	296.041 254(67)	3	1	2	B_2	251.301 459(67)
168.1638(50)	8.7250×10^{-2}	4	2	3	B_1	419.4653(50)	3	1	2	B_2	251.301 459(67)
115.73401(13)	1.5816×10^{-2}	4	1	3	A_2	399.049 356(97)	3	2	2	A_1	283.315 346(94)
240.0720(50)	2.4471×10^{-1}	4	3	1	A_2	523.3873(50)	3	2	2	A_1	283.315 346(94)
21.2099(50)	6.8544×10^{-6}	4	1	4	B_2	317.2512(50)	3	2	1	B_1	296.041 254(67)

Excerpts from the H_3^+ and D_3^+ states files are provided in Table 8. Similarly, the states files for H_2D^+ and D_2H^+ contain the same set of quantum number columns and excerpts for them are shown in Table 9.

All entries in the new states files are marked with a source tag, indicating the method that was used to determine the final term energy for that level. Several values for the source tag can occur in ExoMol line lists (Bowesman et al. 2021) but only three are in use here: 'Ma' for MARVELized energies, 'EH' for energies from effective Hamiltonian calculations and 'Ca' for energies calculated using DVR3D. For all levels marked 'Ca' in all four states files, an uncertainty estimate was calculated using equation (2).

All new and updated states files are ordered on increasing J, Γ_{rve}, and energy. The existing H_2D^+ states file was already formatted this

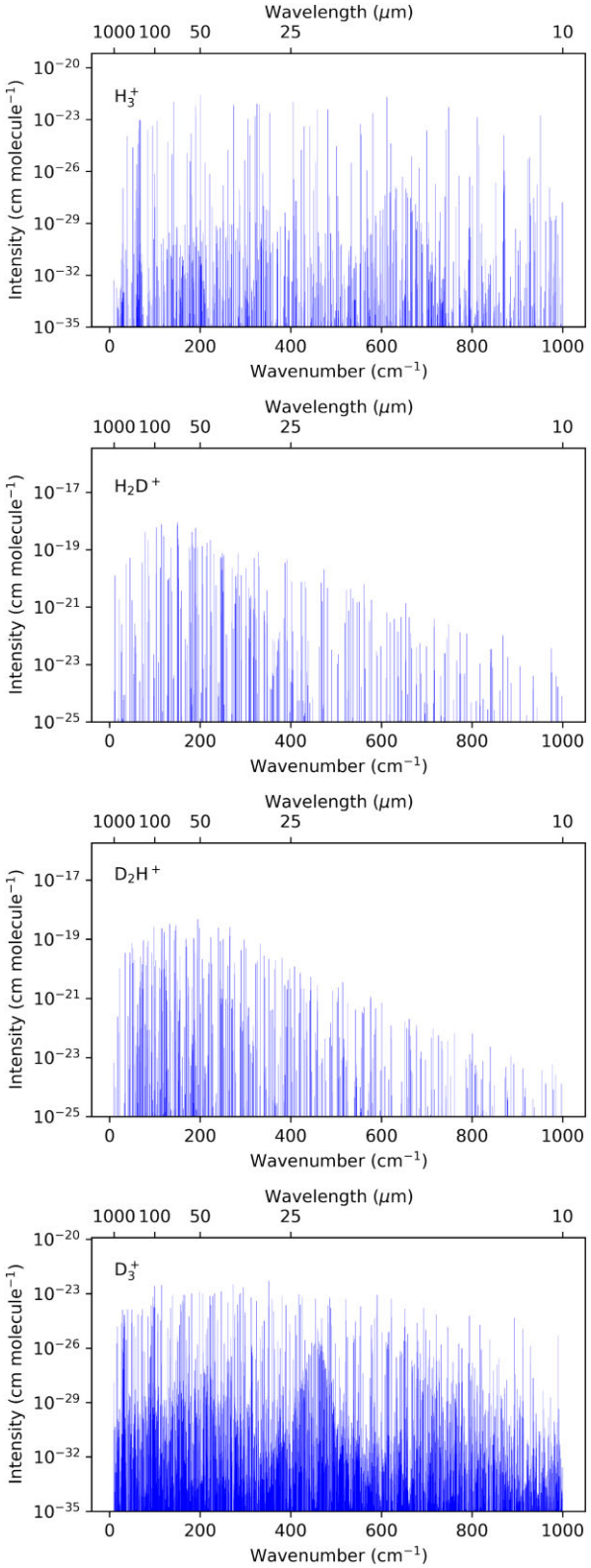

Figure 1. Far infrared spectra for H_3^+ and its deuterated isotopologues, computed using the program EXOCROSS (Yurchenko et al. 2018) at 200 K between 10 and 1000 cm^{-1} (1–10 μm).

way, while H_3^+ was not and has been changed. Hence for H_3^+, the state counting number assigned to each level has been reassigned and the references to these values in the corresponding trans file have accordingly been updated. Excerpts from the trans files for the new D_2H^+ and D_3^+ line lists can be seen in Table 10.

In general, all molecular states should be characterized by three rigorous quantum numbers: J, parity, and the overall symmetry, which also determines the nuclear spin state (ortho/para/meta). All calculations have J and parity rigorously determined; due to the full treatment by DVR3D of the C_{2v} symmetry, the symmetry and nuclear spin statistics are also correctly determined for H_2D^+ and D_2H^+. This is not the case for H_3^+ and D_3^+ however, as the program does not include a full treatment for a D_{3h} Hamiltonian. The symmetry was initially output for all molecular species considered here under C_{2v} symmetry, but was subsequently mapped to the appropriate D_{3h} representation for H_3^+ and D_3^+ for states with quantum number assignments. Due to the nuclear spin statistical weight of the A_1', A_1'' symmetries in H_3^+ being 0, it was possible to map all of the C_{2v} symmetries to the appropriate D_{3h} representation (Mizus et al. 2017). For D_3^+, where D_{3h} symmetry and quantum number assignment was not carried out, the entries retain the C_{2v} symmetries output by DVR3D. These C_{2v} symmetries are given as lower case in the states file, to avoid confusion between the A_1 and A_2 irreducible representations under C_{2v} symmetry (formatted as 'a1' and 'a2') and the A_1', A_1'', A_2', and A_2'' irreducible representations under D_{3h} symmetry.

3.6 Partition Functions

Calculating the partition functions of the new line lists requires the determination of the total degeneracy of each state considered, as show in equation (3)

$$z = \sum_i g_{\mathrm{tot},i} exp\left(-\frac{E_i}{k_\mathrm{B}T}\right), \tag{3}$$

where g_{tot} is the total degeneracy of the ith level, E_i its energy, k_B is the Boltzmann constant, and T is the temperature. The total degeneracy of a level depends directly on the nuclear spin statistical weight, g_{ns}

$$g_{\mathrm{tot}} = g_{\mathrm{ns}}\,(2J+1)\,. \tag{4}$$

The nuclear spin statistical weights represent the number of nuclear spin functions that yield each symmetry. We follow the ExoMol and HITRAN convention of including the full nuclear spin degeneracy in our partition functions. In the case of H_3^+, where each atom consists of one proton with $I = \frac{1}{2}$, Fermi statistics apply which results in no allowed configurations corresponding to the A_1' or A_1'' representations. Accordingly, the g_{ns} values for these representations of H_3^+ are 0, as shown in Table 1. For D_3^+ however, each Deuterium atom has $I = 1$ and is hence a boson, meaning additional representations can occur that give rise to the 'meta' nuclear spin isomer.

Our mappings of the C_{2v} representations output by DVR3D to the full D_{3h} symmetry are complete for all states presented in the H_3^+ line list, but not for the states of D_3^+. Hence, we must also consider the appropriate statistical weights to use when determining the degeneracy of the D_3^+ states left with C_{2v} symmetries. As the D_{3h} representations, A_1', A_1'', A_2', A_2'', E', E'' correspond to A_1, A_2, B_2, B_1, $A_1 \oplus B_2$, $A_2 \oplus B_1$, respectively, under C_{2v} symmetry, we can calculate population weighted average statistical weights for each C_{2v} representation. These are calculated knowing that approximately two thirds of all D_3^+ levels will be E' and E'', due to the constraint that A_1', A_1'', A_2', and A_2'' levels only occur when $G = 3n$, where n

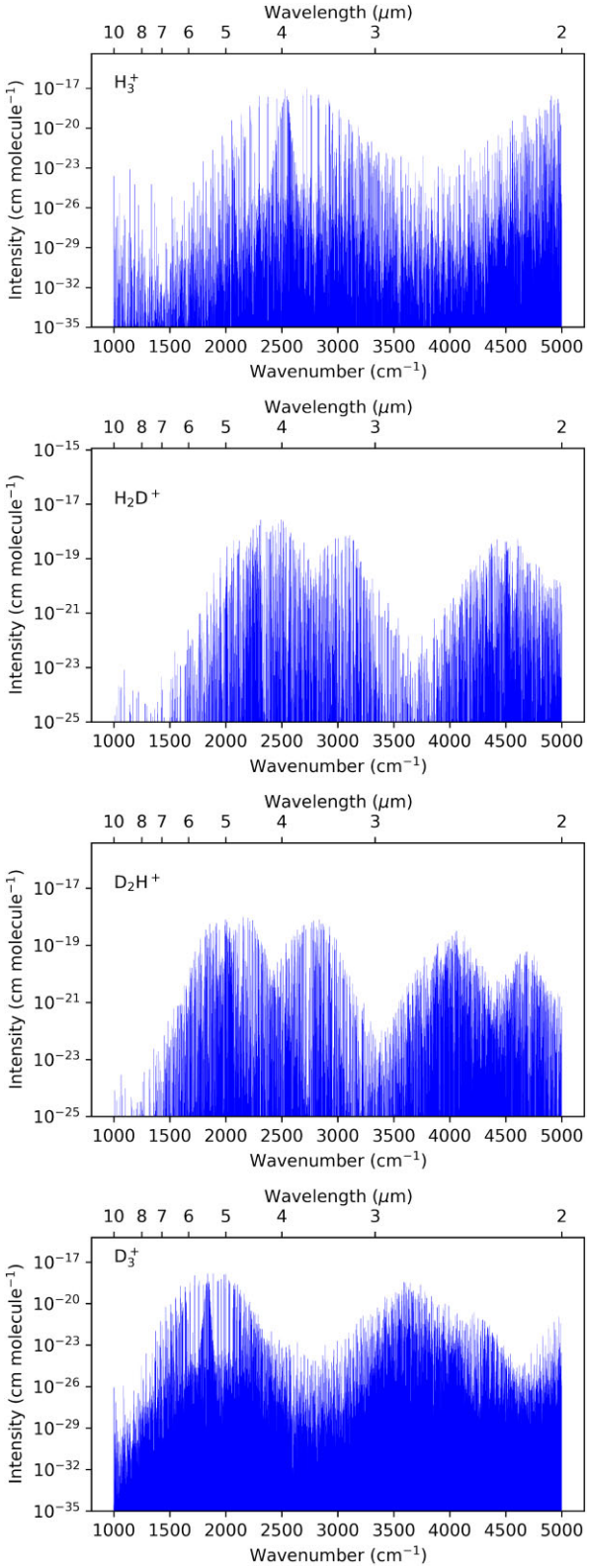

Figure 2. Mid infrared spectra for H_3^+ and its deuterated isotopologues, computed using the program EXOCROSS (Yurchenko et al. 2018) at 200 K between 1000 and 5000 cm^{-1} (10–2 μm).

is an integer (see also Berblinger et al. 1992). Accordingly, for the A_1 and A_2 representations in C_{2v} symmetry, one third will be A_1' or A_1'' under D_{3h} symmetry while the remaining two thirds will be E' and E''. The equivalent population ratio is true for B_1 and B_2 states and the corresponding A_2' and A_2'' representations. These population ratios are then weighted using the weights from Table 1, yielding the g_{ns} values shown in Table 11. These adjusted weights were used to calculate the total degeneracies of the states of the D_3^+ line list for which C_{2v} symmetries are used and are included in the new states file.

Partition functions are given in Table 12 for a series of temperatures up to the value of T_{max} for each line list. Partition functions for D_3^+ had previously been calculated by Ramanlal & Tennyson (2004) and their values are in close agreement with those presented here. For H_2D^+, however, the partition functions differ from those given by Sochi & Tennyson (2010). This is due to the different nuclear spin statistical weights used in their earlier work that did not consider the spin of the Deuterium atom. The degeneracies given in the H_2D^+ line list have been updated to use the nuclear spin statistical weights quoted in Table 1 and are thus consistent with the partition function computed using equation (3) and the same convention.

4 SPECTRA

4.1 Rotational spectra

Purely rotational transitions within the vibrational ground states are important for detections of H_3^+ and particularly its deuterated isotopologues in the interstellar medium. This is due to the low temperatures in such regions driving the majority of the level populations to low-energy states. Predicted transition frequencies for such transitions are given in Table 13 for H_3^+ and D_3^+ and in Table 14 for H_2D^+ and D_2H^+, based on the term energies derived from the MARVEL networks presented here. While the purely rotational transitions of H_3^+ are 'forbidden' due to the lack of a permanent electric dipole moment, it is believed that a small, temporary dipole moment can be induced due to the distortion of the molecule from equilibrium geometry under rotation about the C_2 molecular axis (Pan & Oka 1986; Miller & Tennyson 1988).

The D_3^+ states file contains 43 extremely long-lived states with radiative lifetimes greater than 10^{10} s and can be considered metastable. In the extreme case, two states are calculated to have radiative lifetimes greater than 10^{18} s, a duration greater than the current age of the universe. All of these metastable states are in the vibrational ground state and have $G = J$ or $G = J - 1$. The same is true for the metastable states of H_3^+, though only one of their radiative lifetimes is in excess of 10^{10} s. In both species, this can cause molecules to become 'trapped' in these states in collision free environments with consequences for both laboratory measurements (Kreckel et al. 2004) and for possible maser action.

4.2 Mid and Far Infrared Spectra

Fig. 1 shows example stick spectra for H_3^+ and its deuterated isotopologues in the far infrared region from 10–1000 cm^{-1}. These spectra were generated using the program EXOCROSS (Yurchenko et al. 2018) and were computed for a temperature of 200 K. The predicted transitions frequencies listed in Tables 13 and 14 that are expected to be of importance in the ISM fall within this range. Likewise, spectra were computed for the mid infrared region between 1000 and 5000 cm^{-1} for all species considered here and are shown in Fig. 2. These cover several wavelength ranges where H_3^+ has been

observed in Jupiter's aurorae, such as the *K*-band region centred at 2.2 μm (Uno et al. 2014) and the L band centred on 3.5 μm (Baron et al. 1991). This also covers the wavelength regions observed using the Jupiter infrared Auroral Mapper (JIRAM) instrument onboard NASA's Juno spacecraft (Dinelli et al. 2019; Migliorini et al. 2019) and those covered by the Near infrared Camera (NIRCam) long-wavelength channel onboard JWST.

Comparisons between computed spectra and real observations cannot be made for H_2D^+, D_2H^+, and D_3^+, as no measured transition intensities have been published. McKellar & Watson (1998) presented infrared absorption spectra of the ν_2 fundamental band of H_3^+ and provided integrated intensities, which were well reproduced by the original line list (Mizus et al. 2017).

5 CONCLUSION

We have updated three MARVEL networks for H_3^+, H_2D^+, and D_2H^+ to include all currently published spectroscopic data for these molecules. We have also performed variational nuclear motion calculations using the program DVR3D for D_2H^+ and D_3^+ to produce the new MiZo line lists. The empirical energy levels derived from the MARVEL networks have been used to update the calculated levels of their respective molecules. This allows for the subset of transitions involving these MARVELized energies to be determined to much higher accuracy, making the use of these line lists well suited for high-resolution spectroscopy. The D_3^+ calculations have been combined with a set of energies derived from effective Hamiltonian calculations computed using experimentally determined molecular constants. Given these effective Hamiltonian constants were derived from transitions in infrared bands, the new D_3^+ line list is best suited for infrared studies. Overall, the new D_3^+ line list is of lower resolution than the other three, due to the lack of MARVELized energy levels.

Hyperfine effects are known to be present in the spectra of H_3^+ and its deuterated isotopologues, due to the nuclear spin of the component protons and deuterons (Jensen et al. 1997). These hyperfine splittings have not yet been observed however in either an astrophysical setting or in the laboratory. Were experiments to be conducted to measure the hyperfine-resolved spectra of the species considered here, it would enable the construction of a hyperfine-resolved MARVEL network and subsequently line lists. Similarly, any further measurements of hyperfine-unresolved spectra could be added to the current MARVEL network to further constrain the resultant empirical energy levels and hence improve the accuracy of the line lists. If a sufficiently large number of spectra were observed for D_3^+ to form a well-connected spectroscopic network, it would enable us to further update the D_3^+ line list with MARVEL energies to a high-resolution standard.

The four line lists presented here, each consisting of a states file and transitions file, are made available via www.exomol.com.

ACKNOWLEDGEMENTS

We thank Tibor Furtenbacher and Attila Császár for supplying the MARVEL4 code and for helpful discussions during the course of this work. This work was supported by the European Research Council (ERC) under the European Union's Horizon 2020 research and innovation programme through Advance grant number 883830 and the UK STFC under grant ST/R000476/1. BP acknowledges support from the US National Science Foundation (CHE-1665370), and the Robert A. Welch Foundation (D-1523). NFZ and OLP acknowledge support by State Project IAP RAS No. 0030-2021-0016. JS is grateful to NKFIH for support (PD142580).

DATA AVAILABILITY

The updated MARVEL input files and resulting output energy levels are given as supporting material. All other data are available via the www.exomol.com website.

REFERENCES

Al-Derzi A. R. et al., 2021, J. Quant. Spectrosc. Radiat. Transfer, 266, 107563
Alijah A., Wolniewicz L., Hinze J., 1995, Mol. Phys., 85, 1125
Amano T., 1985, J. Opt. Soc. Am. B, 2, 790
Amano T., 2006, Phil. Trans. Royal Soc. A, 364, 2943
Amano T., Hirao T., 2005, J. Mol. Spectrosc., 233, 7
Amano T., Watson J. K. G., 1984, J. Chem. Phys., 81, 2869
Amano T., Chan M. C., Civis S., McKellar A. R. W., Majewski W. A., Sadovskii D., Watson J. K. G., 1994, Can. J. Phys., 72, 1007
Asvany O., Hugo E., Schlemmer S., Muller F., Kuhnemann F., Schiller S., Tennyson J., 2007, J. Chem. Phys., 127, 154317
Asvany O., Ricken O., Müller H.-S.-P., Wiedner M.-C., Giesen T.-F., Schlemmer S., 2008, Phys. Rev. Lett., 100, 233004
Ballester G. E., Miller S., Tennyson J., Trafton L. M., Geballe T. R., 1994, Icarus, 107, 189
Baron R., Joseph R. D., Owen T., Tennyson J., Miller S., Ballester G. E., 1991, Nature, 353, 539
Bawendi M. G., Rehfuss B. D., Oka T., 1990, J. Chem. Phys., 93, 6200
Berblinger M., Schlier C., Tennyson J., Miller S., 1992, J. Chem. Phys., 96, 6842
Berg M., Wolf A., Petrignani A., 2012, Phil. Trans. Royal Soc. A, 370, 5028
Bergeron P., Ruiz M. T., Leggett S. K., 1997, ApJS, 108, 339
Bogey M., Demuynck C., Denis M., Destombes J. L., Lemoine B., 1984, A&A, 137, L15
Bowesman C. A., Shuai M., Yurchenko S. N., Tennyson J., 2021, MNRAS, 508, 3181
Bowesman C. A., Akbari H., Hopkins S., Yurchenko S. N., Tennyson J., 2022, J. Quant. Spectrosc. Radiat. Transfer, 289, 108295
Caselli P., van der Tak F. F. S., Ceccarelli C., Bacmann A., 2003, A&A, 403, L37
Chadney J. M., Galand M., Koskinen T. T., Miller S., Sanz-Forcada J., Unruh Y. C., Yelle R. V., 2016, A&A, 587, A87
Chen W., Poirier B., 2006a, J. Comput. Phys., 219, 185
Chen W., Poirier B., 2006b, J. Comput. Phys., 219, 198
Chen W., Poirier B., 2010a, J. Theor. Comput. Chem., 9, 825
Chen W., Poirier B., 2010b, J. Parallel Distrib. Comput., 70, 779
Crabtree K. N., Hodges J. N., Siller B. M., Perry A. J., Kelly J. E., Jenkins P. A., McCall B. J., 2012, Chem. Phys. Lett., 551, 1
Császár A. G., Furtenbacher T., 2011, J. Mol. Spectrosc., 266, 99
Dinelli B. M., Neale L., Polyansky O. L., Tennyson J., 1997, J. Mol. Spectrosc., 181, 142
Dinelli B. M., Adriani A., Mura A., Altieri F., Migliorini A., Moriconi M. L., 2019, Phil. Trans. Royal Soc. A, 377, 20180406
Drossart P. et al., 1989, Nature, 340, 539
Fábri C., Mátyus E., Császár A. G., 2011, J. Chem. Phys., 134, 074105
Farnik M., Davis S., Kostin M. A., Polyansky O. L., Tennyson J., Nesbitt D. J., 2002, J. Chem. Phys., 116, 6146
Foster S. C., McKellar A. R. W., Peterkin I. R., Watson J. K. G., Pan F. S., Crofton M. W., Altman R. S., Oka T., 1986a, J. Chem. Phys., 84, 91
Foster S. C., McKellar A. R. W., Watson J. K. G., 1986b, J. Chem. Phys., 85, 664
Furtenbacher T., Császár A. G., 2012, J. Quant. Spectrosc. Radiat. Transfer, 113, 929
Furtenbacher T., Császár A. G., Tennyson J., 2007, J. Mol. Spectrosc., 245, 115
Furtenbacher T., Szidarovszky T., Mátyus Edit Fábri C., Császár A. G., 2013a, J. Chem. Theory Comput., 9, 5471
Furtenbacher T., Szidarovszky T., Fábri C., Császár A. G., 2013b, Phys. Chem. Chem. Phys., 15, 10181
Geballe T. R., Oka T., 1996, Nature, 384, 334

Geballe T. R., Jagod M. F., Oka T., 1993, ApJ, 408, L109
Gibbs A., Fitzgerald M. P., 2022, AJ, 164, 14
Gottfried J. L., McCall B. J., Oka T., 2003, J. Chem. Phys., 118, 10890
Guan Y.-C., Chang Y.-H., Liao Y.-C., Peng J.-L., Wang L.-B., Shy J.-T., 2018, J. Chem. Phys., 148, 124310
Harju J. et al., 2017, ApJ, 840, 63
Hewitt A. J., Doss N., Zobov N. F., Polyansky O. L., Tennyson J., 2005, MNRAS, 356, 1123
Hirao T., Amano T., 2003, ApJ, 597, L85
Hlavenka P., Korolov I., Plasil R., Varju J., Kotrik T., Glosik J., 2006a, Czech. J. Phys., 56, B749
Hlavenka P., Plasil R., Bano G., Korolov I., Ramanlal J., Tennyson J., Glosik J., Gerlich D., 2006b, Int. J. Mass Spectrom., 255–256, 170
Hodges J. N., Perry A. J., Jenkins II P. A., Siller B. M., McCall B. J., 2013, J. Chem. Phys., 139, 164201
Hougen J. T., 1962, J. Chem. Phys., 37, 1433
Indriolo N., McCall B. J., 2012, ApJ, 745, 91
Jaquet R., 2022, J. Mol. Spectrosc., 384, 111585
Jensen P., Paidarová I., Špirko V., Sauer S. P. A., 1997, Mol. Phys., 91, 319
Jusko P., Konietzko C., Schlemmer S., Asvany O., 2016, J. Mol. Spectrosc., 319, 55
Jusko P., Toepfer M., Mueller H. S. P., Ghosh P. N., Schlemmer S., Asvany O., 2017, J. Mol. Spectrosc., 332, 33
Kao L., Oka T., Miller S., Tennyson J., 1991, ApJS, 77, 317
Khodachenko M. L., Shaikhislamov I. F., Lammer H., Prokopov P. A., 2015, ApJ, 813, 50
Koskinen T. T., Aylward A. D., Miller S., 2007, Nature, 450, 845
Kreckel H., Schwalm D., Tennyson J., Wolf A., Zajfman D., 2004, New J. Phys, 6, 151
Kreckel H., Bing D., Reinhardt S., Petrignani A., Berg M. H., Wolf A., 2008, J. Chem. Phys., 129, 164312
Lam H. A., Miller S., Joseph R. D., Geballe T. R., Trafton L. M., Tennyson J., Ballester G. E., 1997, ApJ, 474, L73
Lee S. S., Ventrudo B. F., Cassidy D. T., Oka T., Miller S., Tennyson J., 1991, J. Mol. Spectrosc., 145, 222
Lenz L. F., Reiners A., Seifahrt A., Kaeufl H. U., 2016, A&A, 589, A99
Lindsay C. M., McCall B. J., 2001, J. Mol. Spectrosc., 210, 60
Lindsay C. M., Rade R. M., Jr, Oka T., 2001, J. Mol. Spectrosc., 210, 51
Lubic K. G., Amano T., 1984, Can. J. Phys., 62, 1886
Majewski W., Marshall M. D., McKellar A., Johns J., Watson J., 1987, J. Mol. Spectrosc., 122, 341
Majewski W. A., Feldman P. A., Watson J. K. G., Miller S., Tennyson J., 1989, ApJ, 347, L51
Majewski W. A., McKellar A. R. W., Sadovskii D., Watson J. K. G., 1994, Can. J. Phys., 72, 1016
Markus C. R., McCall B. J., 2019, J. Chem. Phys., 150, 214303
Markus C. R., McCall B. J., Schrader A. W., Esposito A. M., Kocheril P. A., 2018, in 73rd International Symposium on Molecular Spectroscopy. p. MG09
Markus C. R., Kocheril P. A., McCall B. J., 2019, J. Mol. Spectrosc., 355, 8
Mátyus E., Czakó G., Császár A. G., 2009, J. Chem. Phys., 130, 134112
Mátyus E., Fábri C., Szidarovszky T., Czakó G., Allen W. D., Császár A. G., 2010, J. Chem. Phys., 133, 034113
McCall B. J., Oka T., 2000, J. Chem. Phys., 113, 3104
McKellar A., Watson J., 1998, J. Mol. Spectrosc., 191, 215
Melin H., Stallard T., Miller S., Lystrup M. B., Trafton L. M., Booth T. C., Rivers C., 2011, MNRAS, 410, 641
Melin H., Fletcher L. N., Stallard T. S., Johnson R. E., O'Donoghue J., Moore L., Donnelly P. T., 2018, MNRAS, 474, 3714
Melin H. et al., 2019, Phil. Trans. Royal Soc. A, 377, 20180408
Merkt F., Hoeveler K., Deiglmayr J., 2022, J. Phys. Chem. Lett.
Migliorini A. et al., 2019, Icarus, 329, 132
Mikosch J., Kreckel H., Wester R., Plašil R., Glosík J., Gerlich D., Schwalm D., Wolf A., 2004, J. Chem. Phys., 121, 11030
Miller S., Tennyson J., 1988, ApJ, 335, 486
Miller S., Achilleos N., Ballester G. E., Lam H. A., Tennyson J., Geballe T. R., Trafton L. M., 1997, Icarus, 130, 57
Miller S., Stallard T., Melin H., Tennyson J., 2010, Faraday Discuss., 147, 283
Miller S., Geballe T. R., Stallard T., Tennyson J., 2020, Rev. Mod. Phys., 92, 035003
Mizus I. I., Alijah A., Zobov N. F., Kyuberis A. A., Yurchenko S. N., Tennyson J., Polyansky O. L., 2017, MNRAS, 468, 1717
Moore L. et al., 2017, Geophys. Res. Lett., 44, 4513
Morong C. P., Gottfried J. L., Oka T., 2009, J. Mol. Spectrosc., 255, 13
Nakanaga T., Ito F., Sugawara K., Takeo H., Matsumura C., 1990, Chem. Phys. Lett., 169, 269
Neale L., Tennyson J., 1995, ApJ, 454, L169
Neale L., Miller S., Tennyson J., 1996, ApJ, 464, 516
Oka T., 1980, Phys. Rev. Lett., 45, 531
Oka T., 1981, Phil. Trans. Royal Soc. A, 303, 543
Oka T., 2006, Proc. Nat. Acad. Sci., 103, 12235
Oka T., Epp E., 2004, ApJ, 613, 349
Owens A., Dooley S., McLaughlin L., Tan B., Zhang G., Yurchenko S. N., Tennyson J., 2022, MNRAS, 511, 5448
Pan F. S., Oka T., 1986, ApJ, 305, 518
Pavanello M. et al., 2012a, Phys. Rev. Lett., 108, 023002
Pavanello M. et al., 2012b, J. Chem. Phys., 136, 184303
Perry A. J., Hodges J. N., Markus C. R., Kocheril G. S., McCall B. J., 2015, J. Mol. Spectrosc., 317, 71
Perry A. J., McCall B. J., Kocheril G. S., Hodges J. N., Markus C. R., 2016, in 71st International Symposium on Molecular Spectroscopy. p. MH03
Petrignani A. et al., 2014, J. Chem. Phys., 141, 241104
Petty C., Poirier B., 2014, Appl. Math., 5, 2756
Polyansky O. L., McKellar A. R. W., 1990, J. Chem. Phys., 92, 4039
Polyansky O. L., Tennyson J., 1999, J. Chem. Phys., 110, 5056
Ramanlal J., Tennyson J., 2004, MNRAS, 354, 161
Röhse R., Kutzelnigg W., Jaquet R., Klopper W., 1994, J. Chem. Phys., 101, 2231
Saito S., Kawaguchi K., Hirota E., 1985, J. Chem. Phys., 82, 45
Sarka J., Poirier B., 2022, Front. Phys.
Sarka J., Das D., Poirier B., 2021, AIP Adv., 11, 045033
Sochi T., Tennyson J., 2010, MNRAS, 405, 2345
Stallard T., Miller S., Melin H., Lystrup M., Cowley S. W. H., Bunce E. J., Achilleos N., Dougherty M., 2008a, Nature, 453, 1083
Stallard T. et al., 2008b, Nature, 456, 214
Stark R., van der Tak F. F. S., van Dishoeck E. F., 1999, ApJ, 521, L67
Tennyson J., Yurchenko S. N., 2012, MNRAS, 425, 21
Tennyson J., Kostin M. A., Barletta P., Harris G. J., Polyansky O. L., Ramanlal J., Zobov N. F., 2004, Comput. Phys. Commun., 163, 85
Tennyson J., Hill C., Yurchenko S. N., 2013, in 6th international conference on atomic and molecular data and their applications ICAMDATA-2012. AIP, New York, p. 186
Tóbiás R., Furtenbacher T., Császár A. G., Naumenko O. V., Tennyson J., Flaud J.-M., Kumard P., Poirier B., 2018, J. Quant. Spectrosc. Radiat. Transfer, 208, 152
Trafton L. M., Geballe T. R., Miller S., Tennyson J., Ballester G. E., 1993, ApJ, 405, 761
Trafton L. M., Miller S., Geballe T. R., Tennyson J., Ballester G. E., 1999, ApJ, 524, 1059
Uno T., Kasaba Y., Tao C., Sakanoi T., Kagitani M., Fujisawa S., Kita H., Badman S. V., 2014, J. Geophys. Res.: Space, 119, 10,219
Uy D., Gabrys C. M., Jagod M., Oka T., 1994, J. Chem. Phys., 100, 6267
Vastel C., Phillips T. G., Yoshida H., 2004, ApJ, 606, L127
Velilla L., Lepetit B., Aguado A., Beswick J. A., Paniagua M., 2008, J. Chem. Phys., 129, 084307
Ventrudo B. F., Cassidy D. T., Guo Z. Y., Joo S., Lee S. S., Oka T., 1994, J. Chem. Phys., 100, 6263
Walmsley C. M., Flower D. R., des Forets G. P., 2004, A&A, 418, 1035
Warner H. E., Conner W. T., Petrmichl R. H., Woods R. C., 1984, J. Chem. Phys., 81, 2514
Watson J. K. G., 1984, J. Mol. Spectrosc., 103, 350
Watson J. K. G., 1994, Can. J. Phys., 72, 702
Watson J. K. G. et al., 1984, Can. J. Phys., 62, 1875
Watson J. K. G., Foster S. C., McKellar A. R. W., 1987, Can. J. Phys., 65, 38

Western C. M., 2017, J. Quant. Spectrosc. Radiat. Transfer, 186, 221
Wu K.-Y., Lien Y.-H., Liao C.-C., Lin Y.-R., Shy J.-T., 2013, Phys. Rev. A, 88, 032507
Xu L., Gabrys C., Oka T., 1990, J. Chem. Phys., 93, 6210
Xu L. W., Rosslein M., Gabrys C. M., Oka T., 1992, J. Mol. Spectrosc., 153, 726
Yonezu T., Matsushima F., Moriwaki Y., Takagi K., Amano T., 2009, J. Mol. Spectrosc., 256, 238
Yu. S., Pearson J. C., Amano T., Matsushima F., 2017, J. Mol. Spectrosc., 331, 6
Yurchenko S. N., Al-Refaie A. F., Tennyson J., 2018, A&A, 614, A131

SUPPORTING INFORMATION

Supplementary data are available at *MNRAS* online.

Please note: Oxford University Press is not responsible for the content or functionality of any supporting materials supplied by the authors. Any queries (other than missing material) should be directed to the corresponding author for the article.

This paper has been typeset from a TEX/LATEX file prepared by the author.

List of astronomical key words (Updated on 2020 January)

This list is common to *Monthly Notices of the Royal Astronomical Society, Astronomy and Astrophysics*, and *The Astrophysical Journal*. In order to ease the search, the key words are subdivided into broad categories. No more than *six* subcategories altogether should be listed for a paper.

The subcategories in boldface containing the word 'individual' are intended for use with specific astronomical objects; these should never be used alone, but always in combination with the most common names for the astronomical objects in question. Note that each object counts as one subcategory within the allowed limit of six.

The parts of the key words in italics are for reference only and should be omitted when the keywords are entered on the manuscript.

General
editorials, notices
errata, addenda
extraterrestrial intelligence
history and philosophy of astronomy
miscellaneous
obituaries, biographies
publications, bibliography
sociology of astronomy
standards

Physical data and processes
acceleration of particles
accretion, accretion discs
asteroseismology
astrobiology
astrochemistry
astroparticle physics
atomic data
atomic processes
black hole physics
chaos
conduction
convection
dense matter
diffusion
dynamo
elementary particles
equation of state
gravitation
gravitational lensing: micro
gravitational lensing: strong
gravitational lensing: weak
gravitational waves
hydrodynamics
instabilities
line: formation
line: identification
line: profiles
magnetic fields
magnetic reconnection
(magnetohydrodynamics) MHD
masers
molecular data
molecular processes
neutrinos
nuclear reactions, nucleosynthesis, abundances
opacity
plasmas
polarization
radiation: dynamics
radiation mechanisms:general
radiation mechanisms: non-thermal
radiation mechanisms: thermal
radiative transfer
relativistic processes
scattering
shock waves
solid state: refractory
solid state: volatile
turbulence
waves

Astronomical instrumentation, methods and techniques
atmospheric effects
balloons
instrumentation: adaptive optics
instrumentation: detectors
instrumentation: high angular resolution
instrumentation: interferometers
instrumentation: miscellaneous
instrumentation: photometers
instrumentation: polarimeters
instrumentation: spectrographs
light pollution
methods: analytical
methods: data analysis
methods: laboratory: atomic
methods: laboratory: molecular
methods: laboratory: solid state
methods: miscellaneous
methods: numerical
methods: observational
methods: statistical
site testing
space vehicles
space vehicles: instruments
techniques: high angular resolution
techniques: image processing
techniques: imaging spectroscopy
techniques: interferometric
techniques: miscellaneous
techniques: photometric
techniques: polarimetric
techniques: radar astronomy
techniques: radial velocities
techniques: spectroscopic
telescopes

Astronomical data bases
astronomical data bases: miscellaneous
atlases
catalogues
surveys
virtual observatory tools

Software
software: data analysis
software: development
software: documentation
software: public release
software: simulations

Astrometry and celestial mechanics
astrometry
celestial mechanics
eclipses
ephemerides
occultations
parallaxes
proper motions
reference systems
time

The Sun
Sun: abundances
Sun: activity
Sun: atmosphere
Sun: chromosphere
Sun: corona
Sun: coronal mass ejections (CMEs)
Sun: evolution
Sun: faculae, plages
Sun: filaments, prominences
Sun: flares
Sun: fundamental parameters
Sun: general
Sun: granulation
Sun: helioseismology
Sun: heliosphere
Sun: infrared
Sun: interior
Sun: magnetic fields
Sun: oscillations
Sun: particle emission
Sun: photosphere
Sun: radio radiation
Sun: rotation
(Sun:) solar–terrestrial relations
(Sun:) solar wind
(Sun:) sunspots
Sun: transition region
Sun: UV radiation
Sun: X-rays, gamma-rays

Planetary systems
comets: general

comets: individual: . . .
Earth
interplanetary medium
Kuiper belt: general

Kuiper belt objects: individual: . . .
meteorites, meteors, meteoroids
minor planets, asteroids: general
minor planets, asteroids: individual: . . .
Moon
Oort Cloud
planets and satellites: atmospheres
planets and satellites: aurorae
planets and satellites: composition
planets and satellites: detection
planets and satellites: dynamical evolution and stability
planets and satellites: formation
planets and satellites: fundamental parameters
planets and satellites: gaseous planets
planets and satellites: general

planets and satellites: individual: . . .
planets and satellites: interiors
planets and satellites: magnetic fields
planets and satellites: oceans
planets and satellites: physical evolution
planets and satellites: rings
planets and satellites: surfaces
planets and satellites: tectonics
planets and satellites: terrestrial planets
planet–disc interactions
planet–star interactions
protoplanetary discs
zodiacal dust

Stars
stars: abundances
stars: activity
stars: AGB and post-AGB
stars: atmospheres
(stars:) binaries *(including multiple)*: close
(stars:) binaries: eclipsing
(stars:) binaries: general
(stars:) binaries: spectroscopic
(stars:) binaries: symbiotic
(stars:) binaries: visual
stars: black holes
(stars:) blue stragglers
(stars:) brown dwarfs
stars: carbon
stars: chemically peculiar
stars: chromospheres
(stars:) circumstellar matter
stars: coronae
stars: distances
stars: dwarf novae
stars: early-type
stars: emission-line, Be
stars: evolution
stars: flare
stars: formation
stars: fundamental parameters
(stars:) gamma-ray burst: general
(stars:) **gamma-ray burst: individual: . . .**
stars: general
(stars:) Hertzsprung–Russell and colour–magnitude diagrams
stars: horizontal branch
stars: imaging
stars: individual: . . .
stars: interiors

stars: jets
stars: kinematics and dynamics
stars: late-type
stars: low-mass
stars: luminosity function, mass function
stars: magnetars
stars: magnetic fields
stars: massive
stars: mass-loss
stars: neutron
(stars:) novae, cataclysmic variables
stars: oscillations *(including pulsations)*
stars: peculiar *(except chemically peculiar)*
(stars:) planetary systems
stars: Population II
stars: Population III
stars: pre-main-sequence
stars: protostars
(stars:) pulsars: general
(stars:) **pulsars: individual: . . .**
stars: rotation
stars: solar-type
(stars:) starspots
stars: statistics
(stars:) subdwarfs
(stars:) supergiants
(stars:) supernovae: general
(stars:) **supernovae: individual: . . .**
stars: variables: Cepheids
stars: variables: Scuti
stars: variables: general
stars: variables: RR Lyrae
stars: variables: S Doradus
stars: variables: T Tauri, Herbig Ae/Be
(stars:) white dwarfs
stars: winds, outflows
stars: Wolf–Rayet

Interstellar medium (ISM), nebulae
ISM: abundances
ISM: atoms
ISM: bubbles
ISM: clouds
(ISM:) cosmic rays
(ISM:) dust, extinction
ISM: evolution
ISM: general
(ISM:) HII regions
(ISM:) Herbig–Haro objects

ISM: individual objects: . . .
(except planetary nebulae)
ISM: jets and outflows
ISM: kinematics and dynamics
ISM: lines and bands
ISM: magnetic fields
ISM: molecules
(ISM:) photodissociation region (PDR)
(ISM:) planetary nebulae: general
(ISM:) **planetary nebulae: individual: . . .**
ISM: structure
ISM: supernova remnants

The Galaxy
Galaxy: abundances
Galaxy: bulge
Galaxy: centre
Galaxy: disc
Galaxy: evolution
Galaxy: formation
Galaxy: fundamental parameters
Galaxy: general
(Galaxy:) globular clusters: general
(Galaxy:) **globular clusters: individual: . . .**
Galaxy: halo
Galaxy: kinematics and dynamics
(Galaxy:) local interstellar matter
Galaxy: nucleus
(Galaxy:) open clusters and associations: general
(Galaxy:) **open clusters and associations: individual: . . .**
(Galaxy:) solar neighbourhood
Galaxy: stellar content
Galaxy: structure

Galaxies
galaxies: abundances
galaxies: active
galaxies: bar
(galaxies:) BL Lacertae objects: general
(galaxies:) **BL Lacertae objects: individual: . . .**
galaxies: bulges
galaxies: clusters: general

galaxies: clusters: individual: . . .
galaxies: clusters: intracluster medium
galaxies: disc
galaxies: distances and redshifts
galaxies: dwarf
galaxies: elliptical and lenticular, cD
galaxies: evolution
galaxies: formation
galaxies: fundamental parameters
galaxies: general
galaxies: groups: general

galaxies: groups: individual: . . .
galaxies: haloes
galaxies: high-redshift

galaxies: individual: . . .
galaxies: interactions
(galaxies:) intergalactic medium
galaxies: irregular
galaxies: ISM
galaxies: jets
galaxies: kinematics and dynamics
(galaxies:) Local Group
galaxies: luminosity function, mass function
(galaxies:) Magellanic Clouds
galaxies: magnetic fields
galaxies: nuclei
galaxies: peculiar
galaxies: photometry
(galaxies:) quasars: absorption lines
(galaxies:) quasars: emission lines
(galaxies:) quasars: general

(galaxies:) **quasars: individual: . . .**
(galaxies:) quasars: supermassive black holes
galaxies: Seyfert
galaxies: spiral
galaxies: starburst
galaxies: star clusters: general

galaxies: star clusters: individual: . . .
galaxies: star formation
galaxies: statistics
galaxies: stellar content
galaxies: structure

Cosmology
(cosmology:) cosmic background radiation
(cosmology:) cosmological parameters
(cosmology:) dark ages, reionization, first stars
(cosmology:) dark energy
(cosmology:) dark matter
(cosmology:) diffuse radiation
(cosmology:) distance scale
(cosmology:) early Universe
(cosmology:) inflation
(cosmology:) large-scale structure of Universe
cosmology: miscellaneous
cosmology: observations
(cosmology:) primordial nucleosynthesis
cosmology: theory

Resolved and unresolved sources as a function of wavelength
gamma-rays: diffuse background
gamma-rays: galaxies
gamma-rays: galaxies: clusters
gamma-rays: general
gamma-rays: ISM
gamma-rays: stars
infrared: diffuse background
infrared: galaxies
infrared: general
infrared: ISM
infrared: planetary systems
infrared: stars
radio continuum: galaxies
radio continuum: general
radio continuum: ISM
radio continuum: planetary systems
radio continuum: stars
radio continuum: transients
radio lines: galaxies
radio lines: general
radio lines: ISM
radio lines: planetary systems
radio lines: stars
submillimetre: diffuse background
submillimetre: galaxies
submillimetre: general
submillimetre: ISM
submillimetre: planetary systems
submillimetre: stars
ultraviolet: galaxies
ultraviolet: general
ultraviolet: ISM
ultraviolet: planetary systems
ultraviolet: stars
X-rays: binaries
X-rays: bursts
X-rays: diffuse background
X-rays: galaxies
X-rays: galaxies: clusters
X-rays: general
X-rays: individual: . . .
X-rays: ISM
X-rays: stars

Transients
(transients:) black hole mergers
(transients:) black hole - neutron star mergers
(transients:) fast radio bursts
(transients:) gamma-ray bursts
(transients:) neutron star mergers
transients: novae
transients: supernovae
transients: tidal disruption events